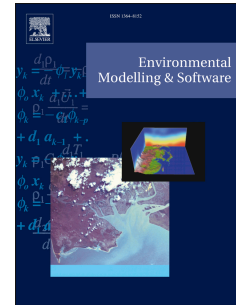


Accepted Manuscript

A web application for hydrogeomorphic flood hazard mapping

Ricardo Tavares da Costa, Salvatore Manfreda, Valerio Luzzi, Caterina Samela,
Paolo Mazzoli, Attilio Castellarin, Stefano Bagli



PII: S1364-8152(18)30795-3

DOI: <https://doi.org/10.1016/j.envsoft.2019.04.010>

Reference: ENSO 4442

To appear in: *Environmental Modelling and Software*

Received Date: 20 August 2018

Revised Date: 12 April 2019

Accepted Date: 18 April 2019

Please cite this article as: Tavares da Costa, R., Manfreda, S., Luzzi, V., Samela, C., Mazzoli, P., Castellarin, A., Bagli, S., A web application for hydrogeomorphic flood hazard mapping, *Environmental Modelling and Software* (2019), doi: <https://doi.org/10.1016/j.envsoft.2019.04.010>.

This is a PDF file of an unedited manuscript that has been accepted for publication. As a service to our customers we are providing this early version of the manuscript. The manuscript will undergo copyediting, typesetting, and review of the resulting proof before it is published in its final form. Please note that during the production process errors may be discovered which could affect the content, and all legal disclaimers that apply to the journal pertain.

A web application for hydrogeomorphic flood hazard mapping

Ricardo Tavares da Costa ^{a, b, *}, Salvatore Manfreda ^c, Valerio Luzzi ^a, Caterina Samela ^{b, c}, Paolo Mazzoli ^a, Attilio Castellarin ^b and Stefano Bagli ^a

^a GECOsistema Srl, Viale Giosuè Carducci, 15, 47521 Cesena, Italy

^b DICAM, University of Bologna, School of Engineering, Viale del Risorgimento, 2, 40136 Bologna, Italy

^c DICEM, University of Basilicata, via Rocco Lazazzera, 75100 Matera, Italy

ABSTRACT

A detailed delineation of flood-prone areas over large regions represents a challenge that cannot be easily solved with today's resources. The main limitations lie in algorithms and hardware, but also costs, scarcity and sparsity of data and our incomplete knowledge of how inundation events occur in different river floodplains. We showcase the implementation of a data-driven web application for regional analyses and detailed (i.e., tens of meters) mapping of floodplains, based on (a) the synthesis of hydrogeomorphic features into a morphological descriptor and (b) its classification to delineate flood-prone areas. We analysed the skill of the descriptor and the performance of the mapping method for European rivers. The web application can be effectively used for delineating flood-prone areas, reproducing the reference flood maps with a classification skill of 88.59% for the 270 major river basins analysed across Europe and 84.23% for the 64 sub-catchments of the Po River.

Keywords:

Data mining

Digital elevation model

Hydrogeomorphology

Large-scale study

Supervised classification

Web application

* Corresponding author. GECOsistema Srl, Viale Giosuè Carducci, 15, 47521 Cesena, Italy (www.gecosistema.com). Tel./Fax: +39 054722619.

E-mail address: ricardotavarescosta@gmail.com (R. Tavares da Costa).

Software and data availability

Software name

Hydrogeomorphic Flood Hazard Mapping

Hardware required

Any web-enabled device with a modern web browser

Software required

Any web browser.

Application components

Geospatial Data Abstraction Library <https://www.gdal.org/>

TauDEM <https://hydrology.usu.edu/taudem/>

scikit-learn <https://scikit-learn.org/>

OpenLayers <https://openlayers.org/>

Highcharts <https://www.highcharts.com/>

MapServer <https://mapserver.org/>

Apache HTTP Server <https://httpd.apache.org/>

Datasets included

EU-DEM <https://land.copernicus.eu/imagery-in-situ/eu-dem/>

Flood hazard maps for Europe <https://data.jrc.ec.europa.eu/dataset/>

CCM River and Catchment Database <http://ccm.jrc.ec.europa.eu/>

Program languages

HTML5, JavaScript and Python

Availability

Users can access the web application via its official website
<http://gecosistema.com/smartflood>

An offline version of the methodological workflow is provided via repository
<http://dx.doi.org/10.17632/pcxmm2hnfw.1>

1. Introduction

According to the European Environment Agency (EEA, 2016), a significant part of the European population is estimated to be living in, or near to, a flood-prone area. This tendency, with historical (e.g., Barredo, 2007) and projected (e.g., Alfieri et al., 2015) consequences of flood disasters tied to it, represents a serious challenge to flood risk management that is also emphasized by the Flood Directive (EU, 2007). Further investments are needed in this field, but authorities and stakeholders also lack prompt and cost-effective solutions to assess and manage every type of flood (e.g. Leskens et al., 2014), particularly over large scales, in contexts where observations are limited and transboundary coordination is required. This is unsatisfactory and to some degree unjustified as today's technological developments provide us with unprecedented quantities of data to develop such solutions (e.g., Ma et al., 2015).

For instance, classical approaches to flood hazard estimation, i.e. the combined use of hydrological and hydrodynamic models (e.g. Şen and Kahya, 2017), are limited by high computational costs when used with massive high-resolution datasets and over large scales (e.g. Schumann, Andreadis et al. 2014). Several authors have tackled this issue either by limiting the quantity and size of the inputs and simplifying the physics of the hydraulic models (e.g. Neal et al., 2012; Alfieri et al., 2014; Dottori et al. 2016) or by resorting to data-driven approaches (e.g. Schumann, Andreadis et al. 2014) or to data mining (e.g., Tehrany et al., 2013, 2014; Rahmati and Pourghasem, 2017).

However, large scale flood hazard mapping using big data, data-mining and artificial intelligence is still something that needs to be comprehensively addressed and that will directly benefit disaster risk reduction and transfer (e.g., insurance, see Jongman et al., 2014; Pappenberger et al., 2015; Ward et al., 2015). At the same time, striving for cost-effective solutions to large scale flood hazard estimation will be decisive to economies and organizations with limited resources and tasked with civil protection and humanitarian aid. We have drawn inspiration from these limitations, to focus on an innovative web-based flood hazard mapping solution that builds upon recently developed geomorphic methodologies (Rennó et al., 2008; Manfreda et al., 2011; Degiorgis et al., 2012; Samela et al., 2017).

Exploiting the potential of such methodologies, a web application named Hydrogeomorphic Flood Hazard Mapping (<http://gecosistema.com/smartflood>, see also Software 1 provided as supplementary material) has been designed as a rather innovative tool. It is presented herein as a demonstrator of the hydrogeomorphic method for flood mapping that makes use of big open-access datasets. The web application was developed to obtain rapid and cost-effective estimates of flood-prone areas outside their original classification domain, in data-scarce or resource limited settings and over large scales. Delineated flood-prone areas will be automatically downscaled to pixel size and from the main stream to the tributaries. The quality of the delineation depends on user choices, from the input layers to the selection of areas for classification and extrapolation.

In particular, our web-based hydrogeomorphic flood hazard mapping environment enables users to: (1) perform a DEM-based flood-prone area delineation; (2) downscale and extrapolate flood studies across Europe; (3) instantly assess mapping performance relative to user-selected reference maps; (4) visualize consistent hydrogeomorphic floodplain delineation at 25 m spatial resolution; and, (5) fine-tune the resulting floodplain mapping on-the-fly via a simple slider. The web application may evolve to a more powerful tool that attends to users' needs and expectations in supporting evidence-based decision making. Examples of similar tools are the Iowa Flood Information System (Demir and Krajewski, 2013) that provides access to flood maps and other flood-related information using an interactive interface or the FLIRE DSS (Kochilakis et al., 2016) that integrates flood maps

with flood warnings, observations and remote sensing data to inform decision makers through a web-based system.

The web application we present here represents a step forward in flood hazard assessment and management and its scientific worth is considered manifold:

- It provides fast and inexpensive estimates of flood-prone areas for specific return periods that complement, but do not replace, results from hydrodynamic simulations.
- It provides fast and inexpensive extrapolation and downscaling capabilities of existing flood studies (e.g., modelling results, remote sensing detection, field surveys), particularly in unstudied areas or tributaries, across political borders and data-scarce regions.
- It can be used to test and conduct experiments with the hydrogeomorphic approach, the classification method and the datasets.
- It enables and exploits collaborative and community-based activities (e.g., Citizen and hydrology working group of the International Association of Hydrological Sciences <https://iahs.info/Commissions--W-Groups/Working-Groups/Candhy.do>).

In order to showcase the (1) operational and (2) scientific capabilities of our web application, we employ it to (1) produce a pan-European flood hazard map for arbitrarily selected return periods, and (2) assess the effectiveness and accuracy of a given geomorphic index for delineating flood-prone areas by using high-resolution, open-access datasets. In particular, our study focuses on two different spatial scales: 270 major river basins in Europe and 64 sub-catchments of the river Po (Italy).

Results presented in this paper reinforce the idea that data-driven approaches are valuable in the handling of big data and for implementation as online tools, while the web technology is a powerful way to bring researchers, developers and end users together, in order to implement innovative approaches and functionalities in the context of large-scale flood assessment and management.

This paper is organized in the following way: 2) review of the progress in hydrogeomorphic methods for flood mapping; 3) description of the geomorphic algorithm for flood hazard mapping adopted within the web application; 4) description of the web application; 5) use of the web application for delineating flood-prone areas across Europe and within the Po river basin and quality assessment of the outputs; 6) discussion.

2. Hydrogeomorphic flood hazard mapping: a review

Simplified data-driven methods for delineating flood-prone areas aim at informing users rapidly in the absence of detailed studies and in data-scarce (e.g., ungauged basins) or resource limited settings, while they enable large-scale analyses without incurring high computational time penalties. In some cases, these methods may not depend explicitly on hydrological conditions nor relate directly to event frequency, duration or magnitude, nor to local settings or antecedent conditions. Instead, they can be based solely on causality between historical floods and the floodplain hydraulic geometry (e.g., Bhowmik et al, 1984).

Leopold and Maddock (1953) evidenced how the water-surface width, mean depth and mean velocity, at different points of the stream channel in a downstream direction, increase on average with discharge as simple power functions. These relationships hold even for very different river systems and tributaries up to bankfull stage. Dodov and Fofoula-Georgiou (2005) provided evidence of two scaling regimes in maximum annual floods, one below and one above the bankfull flow. The authors confirmed that inundation depth was proportional to bankfull depth at any given scale and that bankfull depth scaled with the contributing area. Based on such findings, Dodov and Fofoula-Georgiou (2006) used a geomorphic approach to delineate the floodplain within regions of similar climatic and geologic conditions. Inundation depth was estimated at points along the stream network using scaling relations of bankfull depth and a regional proportionality coefficient. Similarly, Nardi et al. (2006) presented a flat-water approach to delineate the floodplain (i.e., simple intersection of a specified flood depth with the surrounding topography). They used a variable stage at each stream pixel from a stream-order averaged, linear scaling relation. The relation was found by generalizing an outlet flood magnitude to each stream pixel, matching it to the discharge obtained from the Manning uniform flow equation with constant roughness, to estimate the stage.

Rennó et al. (2008) and Gharari et al. (2011) found that, similarly to the topographic wetness index by Beven and Kirkby (1979), the elevation difference to the nearest stream (or incision, as defined by Bhowmik, 1984) previously used to characterize valley-bottom settings (Williams et al., 2000) was correlated to soil water content distribution. Manfreda et al. (2011) specifically investigated the correlation between the topographic wetness index and flood-prone areas and proposed a tailored version of the index by weighing the local upslope contributing area. Flood-prone areas were delineated by searching for the optimal combination of weight and index threshold that would minimize the sum of false negatives and false positives, in relation to a reference flood hazard map.

Degiorgis et al. (2012) proposed the use of a linear binary classification to extrapolate hazard information from a training area to the entire river basin, by searching for the optimal morphological descriptor threshold, relative to a reference flood hazard map for a given return period. Among the tested classifiers, the elevation difference and the distance to the nearest stream were found to be the best performing ones.

Manfreda et al. (2014) compared the linear binary classification, using the modified topographic index and the indices introduced by Degiorgis et al. (2012) to the hydrogeomorphic approach of Nardi et al. (2006). Their study confirmed that the classification using the elevation difference to the nearest stream (i.e., HAND) was reliable for delineating flood-prone areas, something also suggested in a remote sensing application of the HAND model by Westerhoff et al. (2011) and later confirmed by Nobre et al. (2016) and by Zheng et al. (2018). Manfreda et al. (2015) and Samela et al. (2016, 2017) further tested the ability of single and composite indices to classify flood-prone areas. The

Geomorphic Flood Index (GFI, Samela et al., 2017), was found to be the best performing and the most consistent index (Manfreda et al., 2015; Samela et al., 2016, 2017).

As alternatives to the classification of flood-prone areas using the GFI, other data mining techniques somewhat relating to this work have been reported in literature, with good results (Tehrany et al., 2013, 2014; Rahmati and Pourghasem, 2017).

3. Methodology

The selected method is based on a morphological descriptor and its use as a linear binary classification feature (Degiorgis et al., 2012); a complete workflow is presented in Fig. 1 and an offline version of it is provided as supplementary material (Software 1).

The workflow starts with terrain analysis of a DEM, i.e., the computation of local slope, flow direction and upslope contributing area using for example TauDEM utilities (Tarboton, 2015), and the transformation of the reference flood study – in our case, the six flood hazard maps for Europe that correspond to a raster of maximum flood depths per return period – into a binary mask. This transformation is achieved by segmentation, using a pre-defined cut-off depth, set to 0.01 m in this work.

The morphological characterization step corresponds to the computation of the selected morphological descriptor from pre-processed terrain analysis layers and to the definition of a classification area (roughly a buffer of about 1 km around the reference), used to avoid some classification shortcomings (e.g., Kubat et al, 1998). The classification of the morphological descriptor is then performed within the classification area established for each river basin or sub-catchment and for each return period, searching for the optimal threshold that better represents the reference. The optimal threshold is subsequently used to segment the morphological descriptor, by flagging all values above or equal to the threshold as flooded, while those below as flood-free, thus obtaining a hydrogeomorphic flood hazard map.

The output map naturally identifies all possible flood-prone areas in a region of interest and according to the DEM, which are often not limited to the flood extents associated with the main channel and tributaries usually found in numerical models. For this reason, we quantify how capable the morphological descriptor is as a classifier within each classification area. In the following sections, a more detailed description of the workflow is presented.

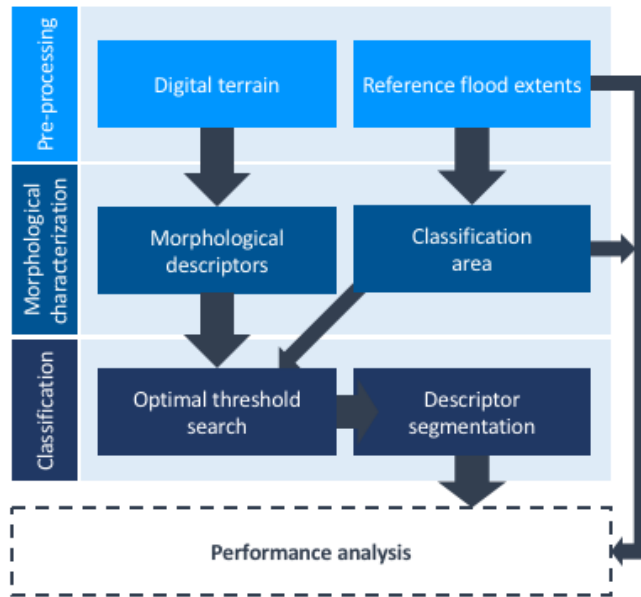


Fig. 1. General methodological workflow for classifying a morphological descriptor and assessing its performance in delineating flood-prone areas. (single-column fitting image)

3.1. Morphological descriptor

The GFI corresponds to the morphological descriptor adopted and used as classifier in the web application; it is a composite index derived directly from terrain analysis and is defined as:

$$GFI_{ij} = \ln(h_{ij}^{ch}/H_{ij}) \quad (1)$$

The GFI is made of two terms, both computed following the steepest downslope D8 flow direction (i.e., the direction towards the eight adjacent neighbours of each pixel). The first term (i, j) consists of an empirically derived stage, h_{ij}^{ch} (in meters), estimated by means of a power law hydraulic scaling relation of bankfull depth (Nardi et al., 2006; Dodov and Fofoula-Georgiou, 2006, Manfreda et al., 2015; Samela et al., 2016, 2017). The stage in each cell is computed using the upslope contributing area A_{kh}^{ch} of each stream channel cell hydrologically connected to the cell i,j (see Fig. 2). The expression is the following:

$$h_{ij}^{ch} = a(A_{kh}^{ch})^n \quad (2)$$

For the sake of simplicity, the power law constant and exponent are assumed transferable and kept with values of $a = 10^{-2}$ and $n = 0.3$ (Nardi et al., 2006; Manfreda et al., 2015), respectively. The second term of the GFI consists of the elevation difference between any given cell z_{ij} , and z_{kh}^{ch} , the nearest connected stream channel cell (or HAND, Rennó et al., 2008; Nobre et al., 2016; Rahmati et al., 2018):

$$H_{ij} = z_{ij} - z_{kh}^{ch} \quad (3)$$

The GFI layer is rescaled before use, with unit value corresponding to the highest hazard level (i.e., near the stream channel) and zero corresponding to the lowest hazard level:

$$GFI_{ij}^* = (GFI_{ij} - GFI^{min}) / (GFI^{max} - GFI^{min}) \quad (4)$$

where GFI_{ij}^* corresponds to the rescaled value and GFI_{ij} the original value in any given cell of the GFI raster. The GFI can effectively be used as a classifier of flood-prone areas (Manfreda et al., 2015; Samela et al., 2016, 2017), fundamentally confining them to the floodplain, i.e. between the active stream channel at bankfull and the surrounding marked topography, noting that, moving away from the channel, H_{ij} increases while the GFI decreases. In Fig. 2, a graphical description of the GFI is presented. To calculate the GFI and subsequently delineate flood-prone areas, steady-state and similar hydrogeomorphic characteristics across scales are assumed.

Finally, we point out that the GFI calculation strictly depends on the prior definition of a stream network. Such network is obtained by imposing a threshold on the area-slope product ($A_{ij}S_{ij}^k$), using a value of 10^5 m^2 and an exponent of $k = 1.7$ (Montgomery and Dietrich, 1989; Giannoni et al., 2005).

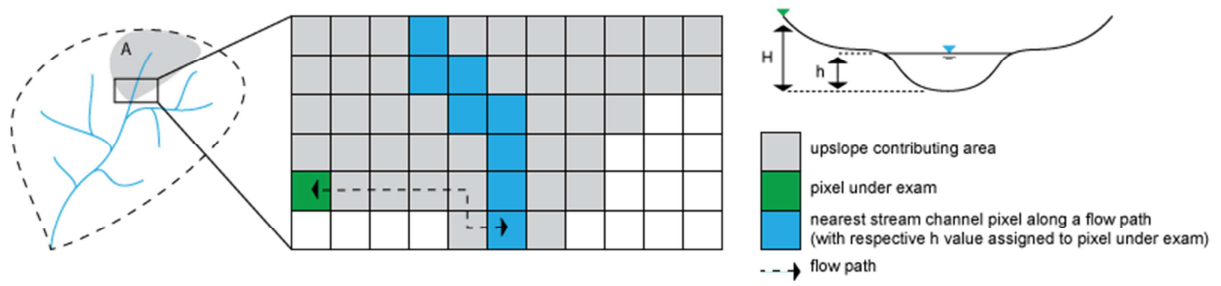


Fig. 2. Description of the Geomorphic Flood Index (GFI), adapted from Manfreda et al., 2015. The left-hand side corresponds to a generic river basin representation, with A the upslope contributing area; in the centre, the raster representation of a zoomed in river basin section; and, on the right-hand side a cross-sectional view of the stream channel and floodplain. (2-column fitting image)

ACCEPTED MANUSCRIPT

3.2. Discrete statistical classification

To delineate flood-prone areas, the dichotomous classification of Degiorgis et al. (2012) is implemented in the web application. The classification consists of a mathematical optimization problem, where the objective is to find the GFI threshold that produces the best possible representation of a reference flood hazard map. Several thresholds are subsequently used to convert the GFI layer to binary and delineate the flood-prone areas. The segmented GFI layer is compared with the reference map for a given return period in order to identify the optimal threshold that matches the maximum of a pre-defined objective function. With this approach, like with any supervised classification exercise (e.g., Kubat et al, 1998), there is a trend towards increased performance when classes are symmetrically distributed. We refer to a classification area, i.e., to a sub-portion of the study domain, corresponding to a fixed buffer (c.a. 1 km) of the reference flood extent with the highest return period, in order to handle class imbalance, namely when pixels of a binary class are greater in number than in the other, within river basins. The classification area allows for discarding the number of flood-free pixels, which are generally in excess.

Performance reported in this work and included as a feature of the web application consists of threshold-dependent measures, one of which is selected as the objective function in the classification stage and another one is selected because of its characteristic of not being affected by class imbalance. Additionally, a receiver operating characteristic (ROC) analysis (Fawcett, 2006) has been performed. In particular, ROC curves and area under the ROC (AUC) were selected as threshold-independent measures.

3.2.1. Threshold-dependent measures

The ideal objective function for the optimization problem of finding the GFI threshold that better discerns between flood-prone and flood-free areas is one that produces the best possible prediction of both true positives and true negatives. The Youden's statistic (Peirce, 1884; Youden, 1950; Stephenson, 2000; Baker and Kramer, 2007; Manzato, 2007), J , also known as true skill statistic, Peirce or Hanssen-Kuipers skill score, can be seen as the probability of making an informed decision with regard to the proportion of correctly predicted classes, assuming false positives to be as undesirable as false negatives. In other words, misclassifying areas that are flood-prone is as serious as misclassifying flood-free areas. For these reasons, and because of its simplicity, smoothness and convergence, the maximization of Youden's J is adopted as a rule in the classification stage of the methodological workflow (Baker and Kramer, 2007). The maximum J value has been used to quantify the success in forecasting dichotomous weather events (e.g., Stephenson, 2000; Manzato, 2007) and in well-known systems, such as the European Flood Alert System (EFAS, Bartholmes et al., 2009) and the Global Flood Awareness System (GloFAS, Alfieri et al., 2012). In this study, the maximum J value defines the optimal GFI threshold for a classification area and return period, i.e., the threshold that best captures the reference flood extent. The Youden's statistic is calculated as:

$$J = \text{tpr} + \text{tnr} - 1 = \text{tpr} - \text{fnr} \quad (6)$$

where tpr is the true positive rate (also called sensitivity, hit-rate or recall, i.e., the probability of a correct hit; Fawcett, 2006), given by:

$$\text{tpr} = 1 - \text{fnr} = \text{tp}/p = \text{tp}/(\text{tp} + \text{fn}) \quad (7)$$

with fnr the false negative rate (or miss rate), tp the number of true positives, i.e., number of flood-prone pixels in both the test and the reference, p the total number of positive samples

and fn the number of false negatives. The true negative rate (or specificity: the probability of a correct miss), tnr , is given by:

$$tnr = 1 - fpr = tn/n = tn/(tn+fp) \quad (8)$$

with fpr being the false positive rate (or fall-out: the probability of an incorrect hit; Fawcett, 2006), tn the number of true negatives (i.e., number of flood-free pixels in both the test and the reference), n the total number of negative samples and fp the number of false positives. The Youden's statistic is determined for all the considered segmentations of the GFI layer during classification; values range from $J = 0$, when a test is useless, to $J = 1$, when perfect. We note that Youden's J maximizes the success of the method but not its utility, i.e. benefits and costs of any particular hydrogeomorphic flood hazard delineation for decision-making purposes are not weighed in (Peirce, 1884; Baker and Kramer, 2007).

The Matthews Correlation Coefficient (Matthews, 1975), MCC, also known as the ϕ -coefficient, was used as a measure of magnitude and direction of the linear relationship between flood-prone areas and the flood hazard maps for Europe, and is given by:

$$MCC = [(tp*tn)-(fp*fn)]/[(tp+fp)*(tp+fn)*(tn+fp)*(tn+fn)]^{1/2} \quad (9)$$

It represents a discrete version of the Person's correlation coefficient (Baldi et al., 2000), specific to dichotomous classification problems. It was chosen as a more balanced overall evaluation of flood-prone areas, due to the full use of the contingency table (tpr , fpr , tnr and fnr) and not sensitive to the class imbalance problem. The MCC is complementary to the more classical performance measures such as the ROC analysis. It indicates how better a given prediction is compared to a random one, taking values of $MCC = -1$ corresponding to a perfect inverse relationship between prediction and reference, to $MCC = 1$ corresponding to a perfect direct relationship between prediction and reference, with $MCC = 0$ representing no relationship between prediction and reference. Other authors have used it to evaluate soil wetness (Ågren et al., 2014) or to resolve cloud structures in satellite imagery (Bley and Deneke, 2013).

3.2.2. Threshold-independent measures

ROC analysis is used to distinguish between decision values in a classifier and their trade-offs between costs and benefits (Swets, 1973, 1988; Bradley, 1997; Fawcett, 2006; Schumann, Vernieuwe et al., 2014). ROC curves are frequently used in flood model performance assessment (e.g., Tehrany et al., 2013, 2014; Schumann, Vernieuwe et al., 2014; Rahmati and Pourghasem, 2017). They provide model performances by plotting together the tpr and the fpr , in this case as a function of the adopted threshold. Each point in the ROC curve represents the comparison of a segmented GFI layer with a reference flood extent. The top left corner of the ROC space represents the perfect classification in terms of correct hits, such that $tpr = 1$ for all values of fpr . Points falling along the diagonal line dividing the ROC space represent a random guess and do not give any useful information regarding the two binary classes. Points falling on the left-hand side are regarded as conservative predictions, while points falling toward the top-right corner classify positives correctly but present a high number of false hits. The optimal operating point in the ROC curve – that represents the optimal GFI threshold for a classification area and return period and that results in the optimal delineation of flood-prone areas – is explicitly determined by the objective function Youden's J described before (Baker and Kramer, 2007). The AUC can be regarded as a general measure of predictive power of the classifier and has been used by several authors, much like the ROC, to assess performance of flood models (e.g., Tehrany et al., 2013, 2014; Schumann, Vernieuwe et al., 2014; Rahmati and Pourghasem, 2017). It comprises a single value ranging from $AUC = 0.5$, poor classifier, to $AUC = 1$, perfect classifier. It represents the probability of ranking a randomly chosen positive instance

higher than a randomly chosen negative (Bradley, 1997; Fawcett, 2006). The AUC is invariant to selected thresholds and prior probabilities (Bradley, 1997; Schumann, Vernieuwe et al., 2014). Provided that a reasonable number of thresholds are considered, the AUC can be estimated by a trapezoidal rule approximation of the definite integral. In our case, the number of thresholds considered can surpass the one million mark, depending on the river basin.

4. Web application and SmartFLOOD platform

We implemented the methodology described in section 3 as a web application that is currently integrated in the SmartFLOOD platform – a cloud-based system that hosts big data, data-driven models and tools and is connected to flexible computing power (Amazon Web Services, <https://aws.amazon.com>). The concept of the platform was inspired by other existing solutions like the Google Earth Engine (<https://earthengine.google.com/>; Gorelick et al., 2017) that brings massive computational capabilities to planetary-scale geospatial analysis as an integrated platform, the Tethys Platform (<https://www.tethysplatform.org/>; Swain et al., 2016) that implements a development and hosting environment for web applications, and the SWATShare platform (Rajib et al., 2016) that establishes a collaborative environment for hydrology research and education. All these web platforms attempt to organize scientific information and operationalize science.

The web application can be used to delineate, downscale and extrapolate flood-prone areas over large areas. Downscaling is interpreted in this work both as the enhancement of spatial detail and as coverage of flood-prone areas. Extrapolation is interpreted as the delineation of flood-prone areas in a river basin, where flood hazard mapping is unavailable, using, for instance, a classification performed in a neighbouring basin, for which detailed outcomes from hydrodynamic studies are available. The low-complexity method employed consists of (a) a synthesis of hydrogeomorphic features into a morphological descriptor, (b) a linear binary classification of the morphological descriptor and (c) the delineation, downscaling, and extrapolation of flood-prone areas.

A version of the web application was developed for the identification of flood-prone areas for the whole Europe and made available online to the general public. The web application enables users to:

- run a supervised classification within a user-selected river sub-catchment, based on one of the reference flood hazard maps for the six return periods considered, retrieve the optimal threshold and classification performance;
- visualize the downscaled and extrapolated flood-prone areas obtained by segmentation of the GFI layer with the optimal threshold;
- manually adjust the GFI threshold on-the-fly, testing its influence on the flood-prone areas;
- get a dynamic response of performance measures that varies with zoom level and window size.

The web application, deployed on a cloud server, uses the static layers described in the following section and employs a number of web-based Geographic Information Systems (GIS) and development software (Swain et al., 2015).

Upload of datasets and download of outputs are currently available for any raster file format supported by the Geospatial Data Abstraction Library (GDAL), visualization is achieved via HTML5 and JavaScript with the help of OpenLayers and Highcharts libraries, while code sharing is done via a Git-type online version-control system.

4.1. Architecture

A cloud-based client-server model is adopted as the web application architecture. The implementation of the web application is illustrated as a network diagram in Fig. 3. The server host functions as a web and file server for restricted uploading and storing of static layers and results, as well as for their retrieval. Clients and server communicate over the internet via any modern web browser. The web application framework incorporates a Web-GIS front-end made of a combination of HTML5 (a markup language) and OpenLayers (an open source JavaScript library), and a server-side, which combines MapServer (an open source geographic data rendering engine) and Apache (an open-source HTTP server). All core model functions are written in Python.

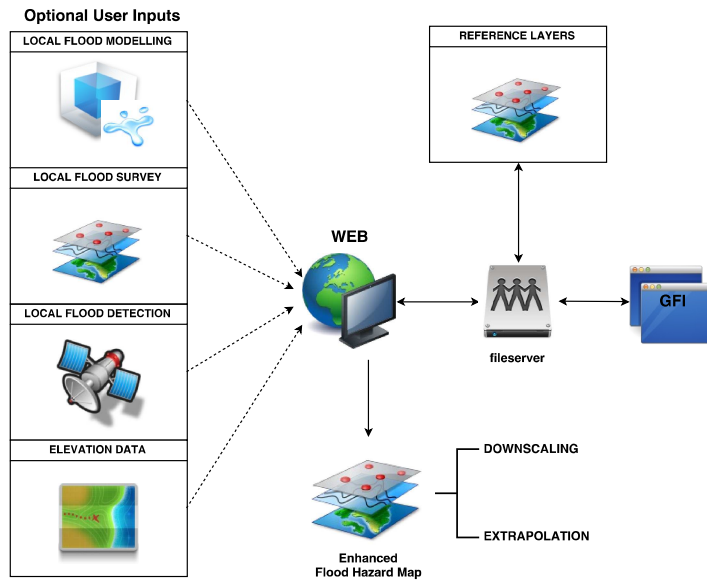


Fig. 3. Client-server diagram showing the implementation of the web application. (1.5-column fitting image)

4.2. Back-end

Web application I/O is done using GDAL and is available in any raster file format supported by this library. The core model functions accessible to users consist of:

1. preparing data for supervised classification;
2. linear binary classification of the morphological descriptor GFI;
3. computation of classification performance measures.

When the user selects a river sub-catchment and return period in the web user interface, the algorithm searches for the corresponding datasets, constricts the layers to the pre-defined classification area and vectorises them.

The classification stage is performed with the help of scikit-learn, a Python library for machine learning functionalities. A number of thresholds are fixed based on the range of values of the bounded GFI layer. For each threshold, statistics are computed and used to calculate the objective function. The algorithm then solves the optimization problem by maximizing the objective function, through retrieval of the corresponding optimal GFI threshold. The final flood-prone areas are delineated within the whole river basin (downscaled extrapolation) to which the classification sub-catchment belongs. The delineation is achieved by optimal threshold segmentation of the GFI layer, which discerns flood-prone from flood-free areas. Finally, within the selected classification area, the flood-prone areas are compared to the reference flood hazard map. Several performance metrics (including, but not limited to the ones used in this paper) are computed and made available to the user. We note that the pre-processing and morphological characterization steps, executed offline to produce the georeferenced static layers, are currently not part of the web application workflow.

4.3. Front-end

The responsive Web-GIS single page front-end is designed to allow users to visualize and interact with the hydrogeomorphic method at the pan-European scale, using any modern web browser. The front-end is built with HTML5, taking advantage of JavaScript, OpenLayers and Highcharts to draw graphics. OpenLayers provides the client-side mapping utilities to handle geospatial data, while Highcharts provides the additional features that complement the interface. The final results are styled and published by the MapServer on the server-side. Fig. 4, shows the web user interface as a step-by-step usage example of the web application (video walkthroughs are also provided as supplementary material, MMC 1 and MMC 2). The web application is implemented in the most user-friendly way possible, enabling users to test the methodology without being concerned about the details behind the system. The user requests the web application core functionality through a simple point-and-click application programming interface, selecting the river sub-catchment and return period of the reference desired to execute the linear binary classification of flood-prone areas. Function returns are made visible to the user through the Web-GIS interface as a combination of interactive maps, summary tables and plots.

As mentioned in section 3 (see subsection 3.2.), the classification of flood-prone areas results in the maximization of the method's success, i.e. finding the threshold that corresponds to the optimal operating point in the ROC curve, although not necessarily its utility (Peirce, 1884; Baker and Kramer, 2007). To address this, we have implemented a slider that allows the user to adjust on-the-fly the rendered optimal flood-prone areas that resulted from the classification stage, so that subjective benefits and costs of a delineation can be taken into account (Baker and Kramer, 2007). Furthermore, a dynamic response of performance measures that varies with zoom level and window size is implemented based on the pixel count of the two critical classes (i.e., flood-prone and flood-free areas),

constricted by the map bounding box. Finally, we took advantage of having static layers in the file server to render maps faster across scales using pre-built tile caching (MapCache).

ACCEPTED MANUSCRIPT

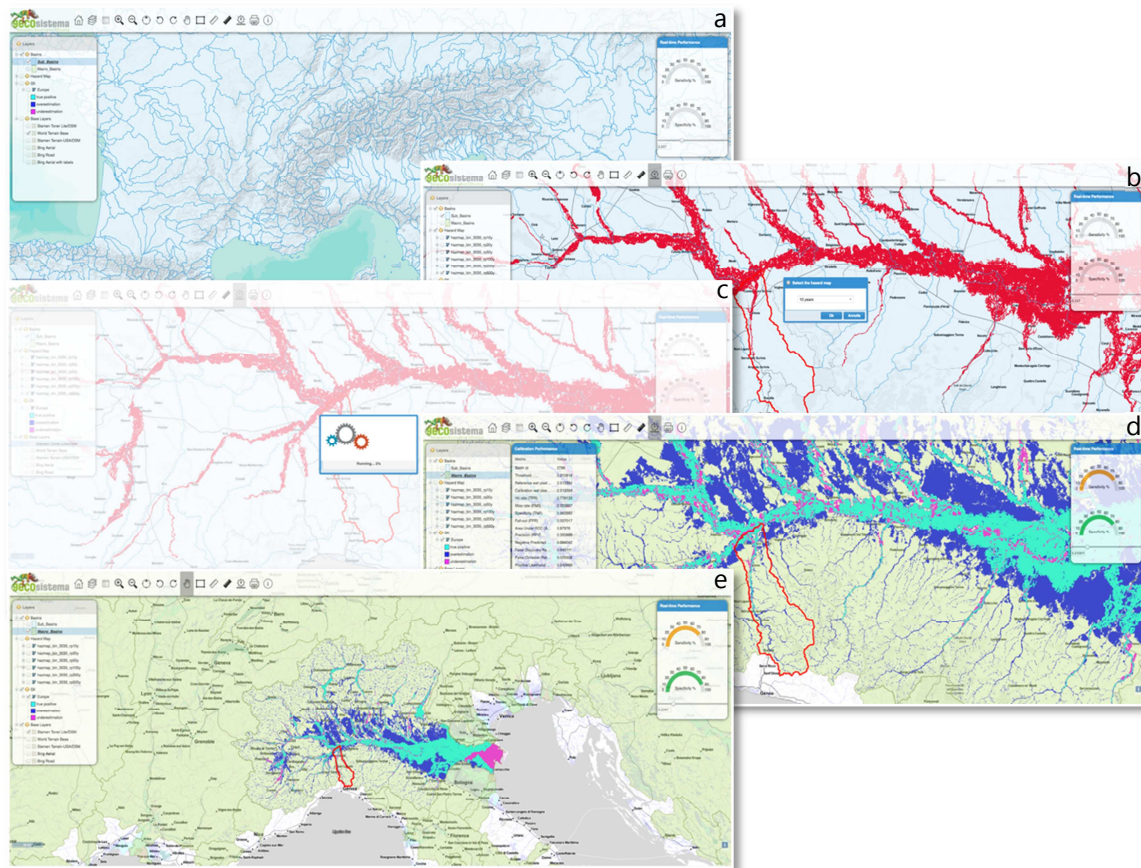


Fig. 4. Usage exemplification of the web application based on the hydrogeomorphic method for delineating flood-prone areas over large scales. a) river sub-catchment selection; b) reference flood map selection, with associated return period; c) classification of morphological descriptor; d) visualization of classification results and performance measures (top-left corner); and, e) downscaled extrapolation of the optimal threshold and delineation of flood-prone areas over the corresponding river basin, with dynamic response of performance (top-right corner). (2-column fitting image)

4.4. Parallelization strategy

The same concurrent programming model is used in different phases of the methodological workflow, from pre-processing and morphological characterization to classification and validation. An exception was made for terrain analysis, which followed a different parallelization strategy, used as an out-of-the-box feature of TauDEM utilities (Tarboton, 2015). The domain is decomposed in logical units (i.e., hydrological unique river basins and sub-catchments) used as natural geometric domain partitions for parallel computation (data parallelism). Decomposition is achieved using utilities from GDAL (OSGeo, 2017) to process the geospatial data. Execution is achieved concurrently and asynchronously, distributing queued data across sub-processes spawned from a pool, carrying out exactly the same independent computations on each partition, minimizing the total execution time and avoiding overload.

5. Large-scale delineation of flood-prone areas

In this section, we present a pan-European application of the web-based tool described in the previous sections, which will serve as the basis for discussing the methodological workflow characterizing the tool and for highlighting its potential capabilities. Additionally, our study provides a useful indication on the reliability of the selected hydrogeomorphic method in flood delineation.

Furthermore, we summarize the results of the array of analyses that can be performed through the platform. In particular, we look at the skill of the GFI as a binary classifier of flood-prone areas. Once the optimal GFI thresholds have been selected, we compare the platform outputs, i.e. the geomorphologic delineated flood-prone areas, to the reference flood hazard maps, looking at the distribution of optimal GFI thresholds, as well as J and MCC values across space, scales and return periods. Finally, we analyse the GFI classification skill through a ROC analysis that can be performed within the platform.

5.1. Datasets and study area

Table 1 lists all the open-access datasets used in our study. The EU-DEM (version 1.0, EEA, 2015, Fig. 5) at approximately 25 m resolution was selected for computing the morphological descriptor. This dataset is freely accessible online through the Copernicus Data and Information Access Services, funded by the European Union. At the easternmost region of Europe, where data is lacking, the EU-DEM was merged with the Shuttle Radar Topography Mission (SRTM – USGS, 2015) 1 arc-second near-global digital elevation data (at approximately 30 m pixel size).

The undefended flood hazard maps for Europe (Dottori et al., 2016a-f, Fig. 6) were selected to estimate the reference flood extents needed in the methodological workflow (see section 3 and Fig. 1). These maps are the only well-known open-access datasets available for the whole region. According to Alfieri et al. (2014), they were produced by simulating a European-wide discharge climatology using the LISFLOOD rainfall-runoff model (van der Knijff et al., 2010), by estimating synthetic design hydrographs from the derived climatology and by simulating floodplain hydrodynamics using the LISFLOOD model using the hydrographs as boundary conditions (Bates et al., 2010; Neal et al., 2011). Hydrodynamic simulations were performed by Alfieri et al. (2014) for every 5 km stretch of the river network (unspecified delineation method) and only for river basins with an upstream area greater than 500 km². As highlighted by Alfieri et al. (2014), the flood hazard maps for Europe are affected by a number of uncertainties and limitations, namely space- and time-resolution issues associated with the inputs (e.g., noise in the DEM and its incapability of resolving flood defences, coarse resolution of meteorological inputs and a tendency of the method to

overestimate runoff). In fact, the flood hazard map for Europe for the 100-year return period event presents hit rates between 59% and 78% and critical success between 43% and 65% evaluated based on specific national/regional hazard maps. Therefore, we are aware of the limitation of such datasets that offer a preliminary description of flood hazard at the European scale. In case new maps become available, they can easily be incorporated in the proposed web application.

In this paper we refer to a study area composed of a selection of 270 river basins (Fig. 7) from the European mainland and continental islands that drain into the Atlantic, the Mediterranean, Black, Baltic and North Seas. Europe's major rivers have a length ranging from approximately 324 km to 2860 km (excluding the Volga) and their river basins are relatively small in area when compared to their counterparts at the global scale, with just 70 European river basins exceeding an area of 10000 km².

Our analyses are summarized at the basin scale, where study catchments have been selected by filtering the Catchment Characterisation and Model (CCM) River and Catchment Database, version 2.1 (de Jager and Vogt, 2010). In particular, we focused on streams with Strahler order (Strahler, 1964) greater or equal to 5, which is consistent with other large-scale studies of fluvial flood hazard (Muis et al., 2015). River basins corresponding to such streams and intersecting a country from the European Economic Area were selected for the evaluation of flood-prone areas.

Selected river basins are characterized by fairly diverse sizes (ranging from 500 to 750000 km², see also Fig. 7), topography (Western Uplands, North European plain, partially underwater, Central Uplands and Alpine Mountains with altitudes surpassing 4500 m), climate (e.g., Kottek et al., 2006; arid in the eastern Iberian Peninsula to warm temperate in most central and northern Europe, boreal in the Pyrenees, Alps and Carpathians, with the last two also presenting a polar climate), and different degrees of anthropization.

In order to explore the impact of basin scale on the proposed methodology, 64 additional sub-catchments of the river Po in Italy (Fig. 8) have been included in the study (with sizes ranging from 1 to 6300 km²).

Table 1

Open-access datasets used in the delineation of flood-prone areas across Europe. (two-column fitting table)

Name		File format	Description	Reference
European Digital Elevation Model (EU-DEM), version 1.0		GeoTIFF raster image	Terrain elevation data for Europe	EEA (2015)
Flood hazard maps for Europe	10-year return period	GeoTIFF raster image	Maximum flood depth data for Europe	Dottori et al. (2016a)
	20-year return period			Dottori et al. (2016b)
	50-year return period			Dottori et al. (2016c)
	100-year return period			Dottori et al. (2016d)
	200-year return period			Dottori et al. (2016e)
	500-year return period			Dottori et al. (2016f)
Catchment Characterisation and Modelling (CCM) River and Catchment Database, version 2.1		Shapefile geospatial vector	Polygon coverage of selected European river basins	de Jager and Vogt, (2010); EC-JRC (2018)

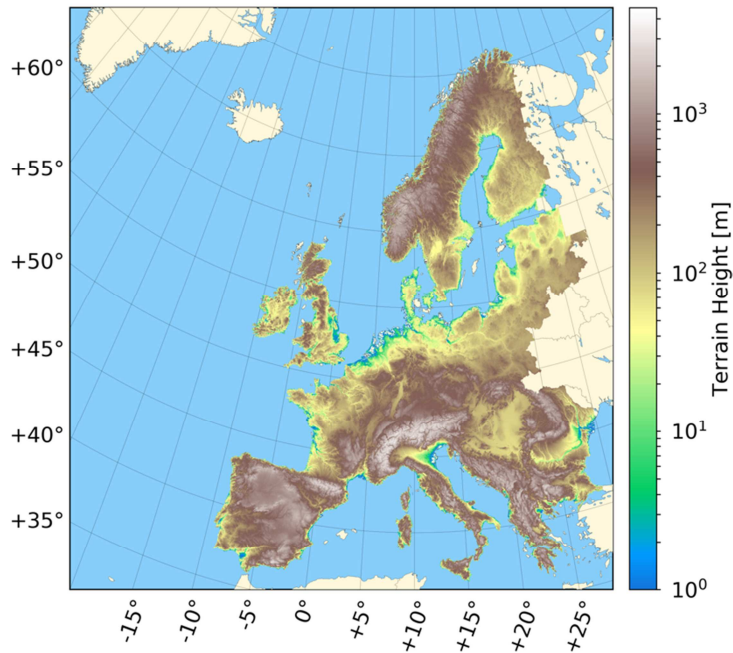


Fig. 5. European digital elevation model (EU-DEM; EEA, 2015) for computing the morphological descriptor. (single-column fitting image)

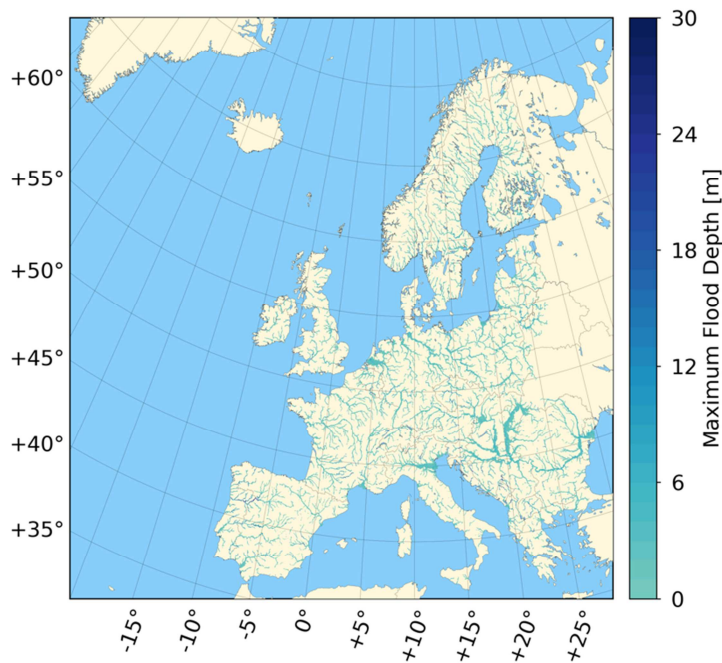


Fig. 6. Flood hazard maps for Europe (e.g., Dottori et al., 2016d) used as reference in the classification of flood-prone areas. (single-column fitting image)

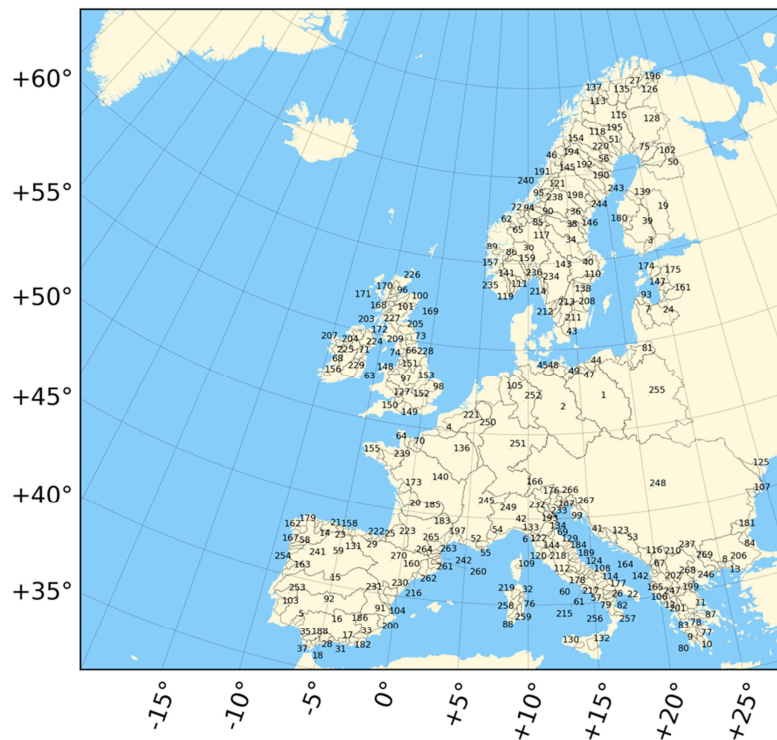


Fig. 7. Study area consisting of 270 major European river basins obtained from the Catchment Characterisation and Model layer, River and Catchment Database (CCM, de Jager and Vogt, 2010). (1.5-column fitting image)

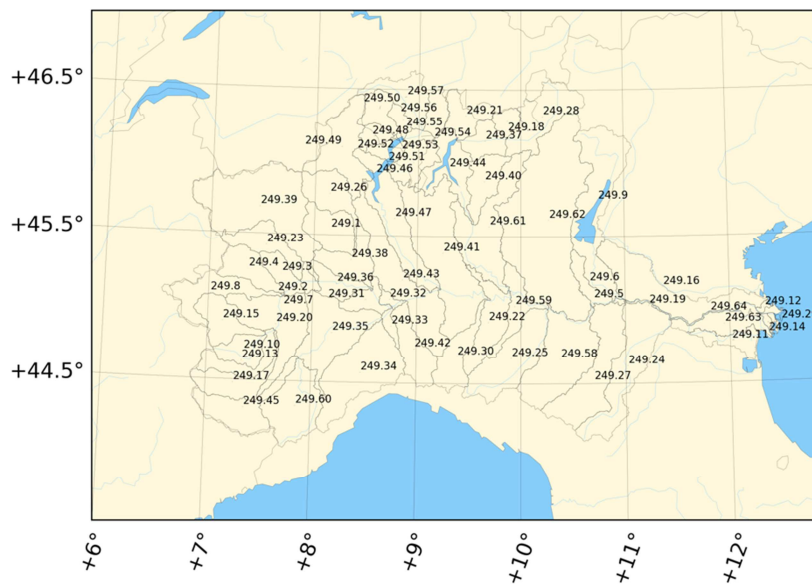


Fig. 8. Study area consisting of 64 sub-catchments of the Po river, Italy, obtained from the Catchment Characterization and Model layer, River and Catchment Database (CCM, de Jager and Vogt, 2010). (1.5-column fitting image)

5.2. Results

5.2.1. Web application generated flood hazard maps

The delineation, downscaling and extrapolation of hydrogeomorphic flood-prone areas can be performed online using the web application. In Fig. 9, we show an output of the web application relative to a specific classification. The figure provides a comparison between the hydrogeomorphic flood-prone areas delineated using the web application (merger of cyan and dark blue pixels) and the reference flood extents derived from the 100-year flood hazard map for Europe (merger of cyan and magenta pixels) from Dottori et al. (2016d). The example refers to a calibrated threshold value of the GFI (Fig. 9a) and a slider operation to control the GFI threshold (Fig. 9b), where the user changes the calibrated threshold and gets an immediate feedback on overestimated (dark blue pixels) and underestimated (magenta pixels) flood-prone areas and how they change visually in the study region or catchment.

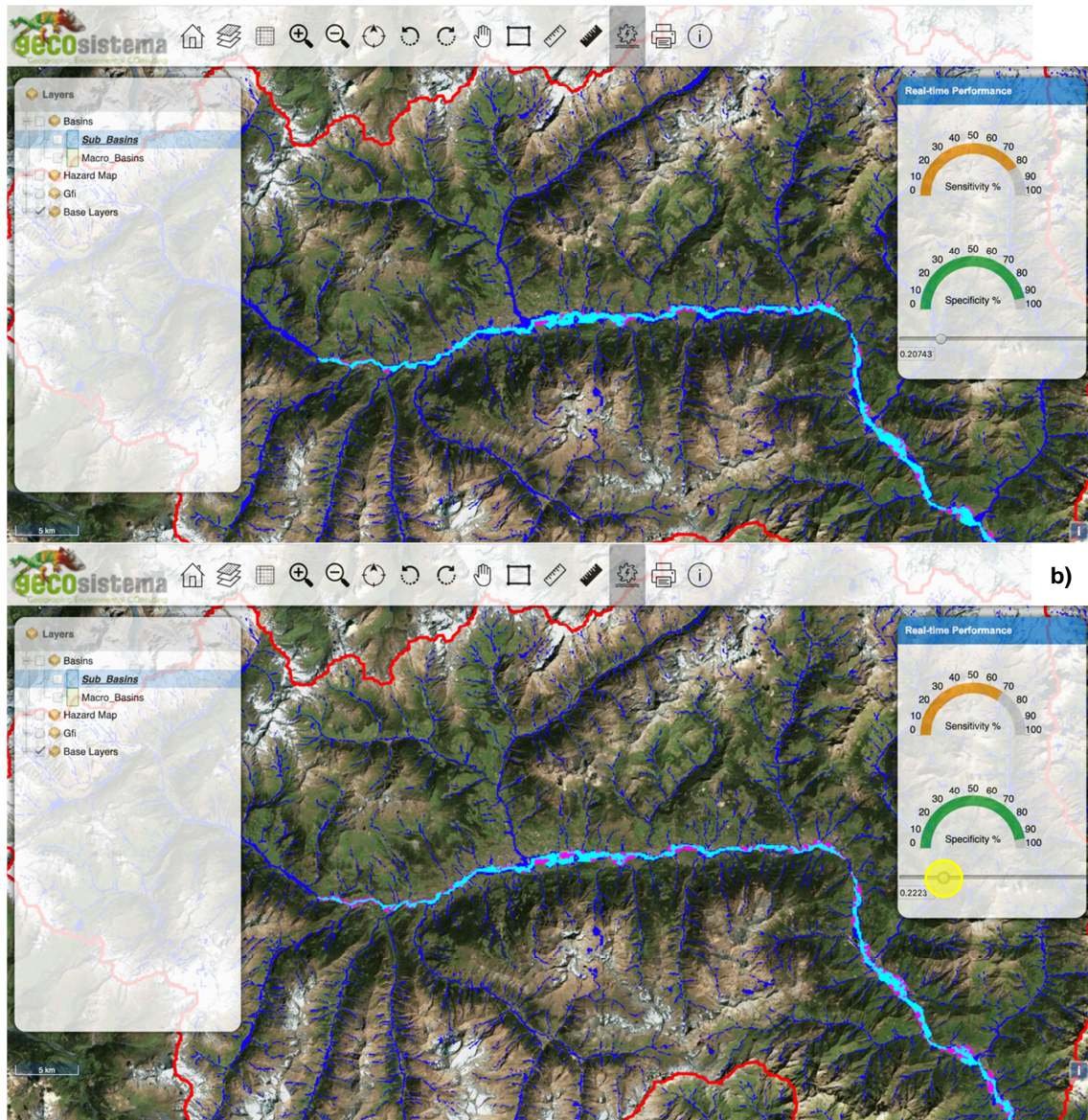


Fig. 9. Sample overlay of the 100-year return period flood hazard map for Europe (Dottori et al., 2016d) on the delineated hydrogeomorphic flood-prone areas using the a) calibrated GFI threshold and b) GFI threshold controlled through slider operation (marked with a yellow circle). (2-column fitting image)

5.2.2. Optimal classifier thresholds and Youden's statistic

The classification of the morphological descriptor GFI within the pre-defined classification area resulted in an optimal GFI threshold for each European river basin, each Po river sub-catchment, and each return period considered. In this section, we compare the delineated and downscaled hydrogeomorphic flood-prone areas with the reference flood hazard maps for Europe, to understand how well the former replicates the latter. We must acknowledge that the aim of such comparison is more to test the potential of the geomorphic procedures rather than to reproduce a perfect match with a reference flood map that contains several approximations.

The resulting spatial distribution of optimal GFI thresholds obtained after the classification step (see Fig. 1), maximizing Youden's J for all major river basins in Europe (Fig. 10 and Fig. 21 in supplementary material) shows low variability. This implies that, at this scale, the optimal threshold is fairly similar across major river basins in Europe. Fig. 11 (and Fig. 22 in supplementary material) shows much higher heterogeneity in terms of the optimal GFI thresholds within the sub-catchments of the river Po: a pattern of higher GFI thresholds can be seen in flatter regions and of lower GFI values in headwater catchments.

The spatial distribution of the maximum Youden's J accounts for the correct identification of the two critical classes, namely flood-prone and flood-free areas, and characterizes the success of the classification. In general, a greater discerning capability of the morphological descriptor GFI will result in high J values. Fig. 12 shows that the spatial distribution of J values within major river basins in Europe is fairly homogeneous, with low variability across return periods (on this point see also Fig. 23 in supplementary material). The variability in the sub-catchments of the river Po is more pronounced (Fig. 13 and Fig. 24 in supplementary material) and shows higher J values for headwater catchments and lower J values in sub-catchments in the lower part of the basin.

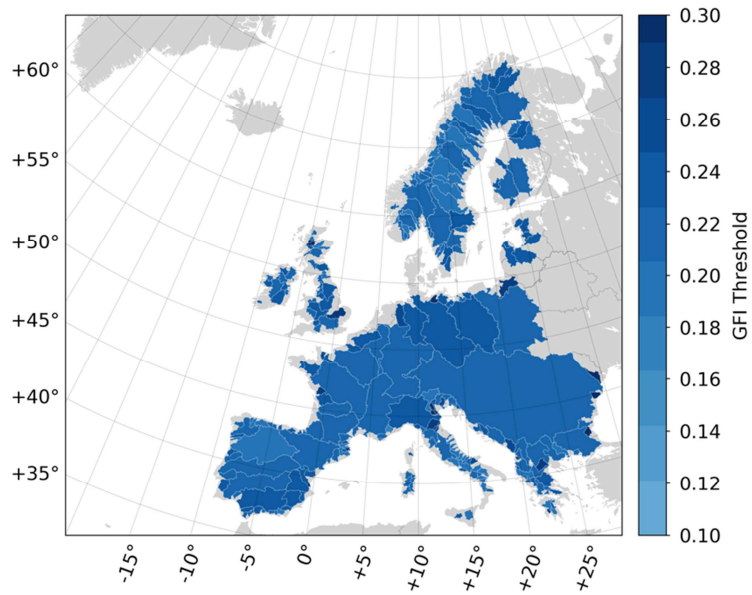


Fig. 10. Spatial distribution of the optimal Geomorphic Flood Index (GFI) threshold for the 100-year return period, within the classification area set for each major river basin in Europe. (single-column fitting image)

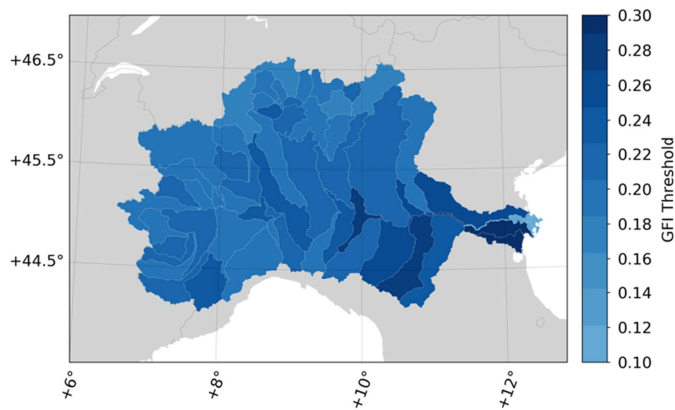


Fig. 11. Spatial distribution of the optimal Geomorphic Flood Index (GFI) threshold for the 100-year return period, within the classification area set for each sub-catchment of the river Po, in Italy. (single-column fitting image)

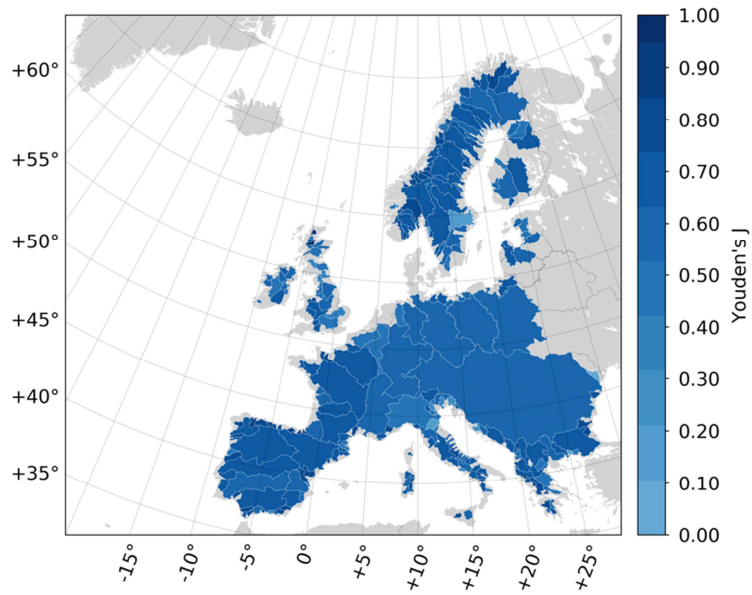


Fig. 12. Spatial distribution of the Youden's statistic (J) for the 100-year return period, within the classification area set for each major river basin in Europe. (single-column fitting image)

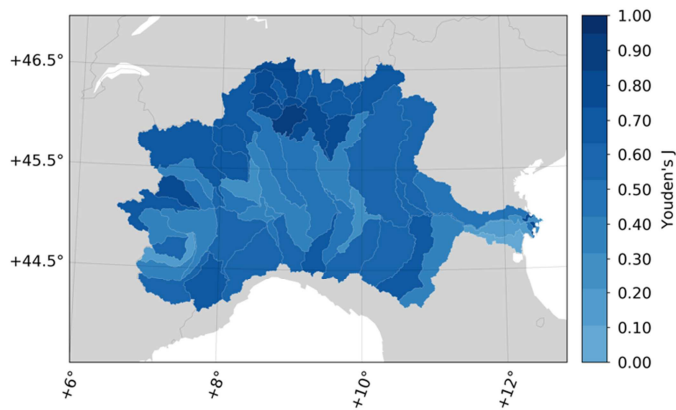


Fig. 13. Spatial distribution of the Youden's statistic (J) for the 100-year return period, within the classification area set for each sub-catchment of the river Po, in Italy. (single-column fitting image)

5.2.3. Analysis of classifier skill

The skill of the GFI-based method is assessed by means of the ROC and AUC obtained within the pre-defined classification areas and is examined for each major river basin in Europe and return period considered (10, 20, 50, 100, 200 and 500-year), as well as for the sub-catchments of the river Po in Italy. In Fig. 14, a sample of ROC curves and respective AUC values are presented, providing an overview of different performances obtained.

Among the 270 river basins analysed herein, some show high discerning capability (i.e., the ROC curve approaches the top left corner and the AUC tends towards unity), while a few underperform, even though they still perform better than random guessing (i.e., curve above the bisecting line of the ROC space and AUC value greater than 0.5). The spatial distribution of AUC values is rather homogeneous with relatively high values in most of the major river basins in Europe (Fig. 15 and Fig. 25 in supplementary material). Also, AUC values show a low variability between different return periods.

Analogously to Youden's J and GFI optimal thresholds, differences between AUC values become more pronounced within the sub-catchments of the river Po and their spatial distribution seems to highlight a greater discerning capability of the morphological descriptor GFI where mountainous areas are prevalent (Fig. 16 and Fig. 26 in supplementary material).

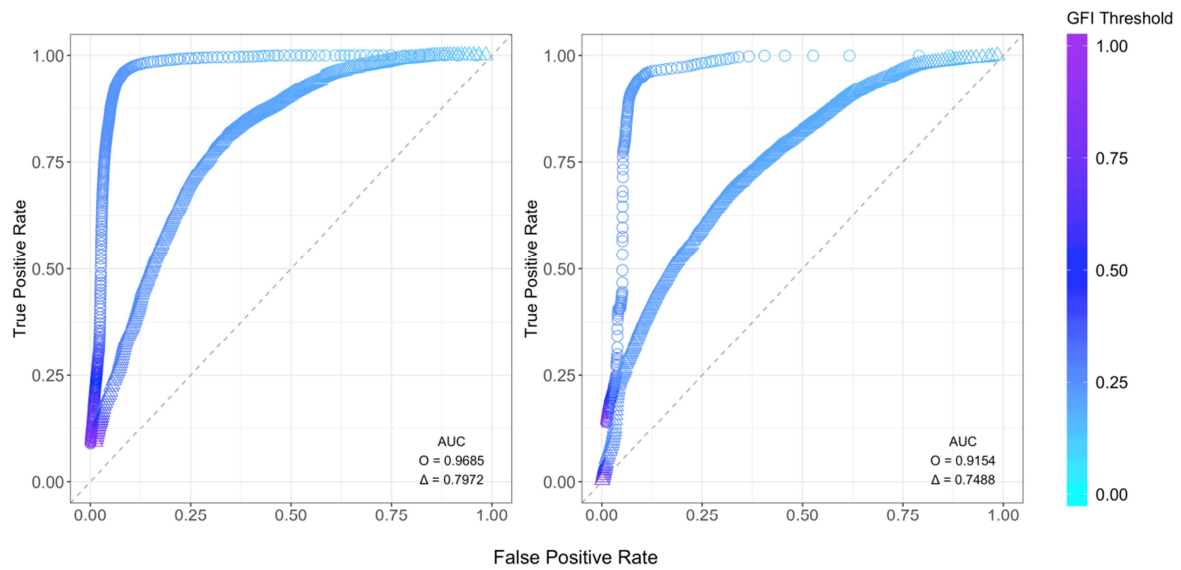


Fig. 14. Discerning capability of the Geomorphic Flood Index (GFI) for the 100-year return period; sample receiver operating characteristic (ROC) curve and respective area under the ROC curve (AUC) values for a good (O) and poor performing river basin (Δ). On the left, two major river basins in Europe and, on the right, two sub-catchments of the River Po, Italy. (2-column fitting image)

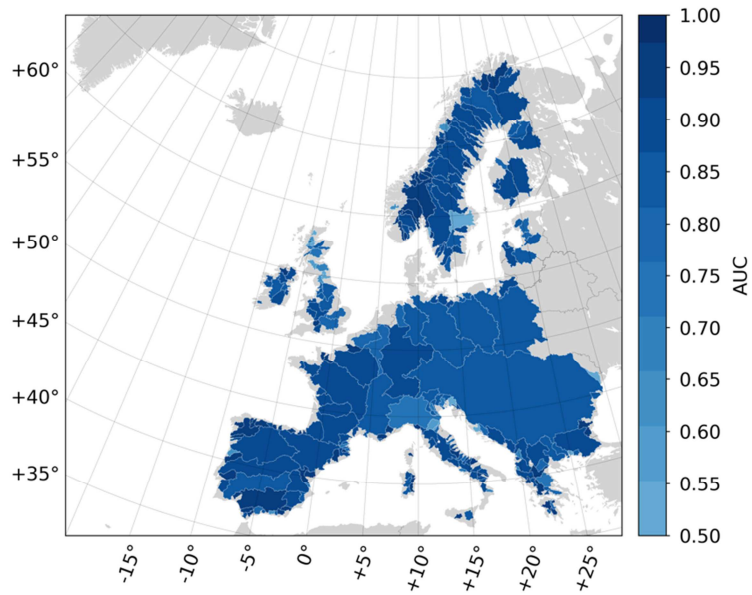


Fig. 15. Spatial distribution of the area under the receiver operating characteristic (AUC) for the 100-year return period, within the classification area set for each major river basin in Europe. (single-column fitting image)

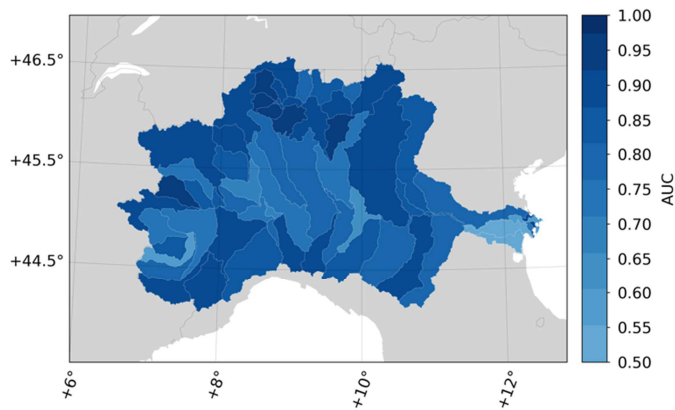


Fig. 16. Spatial distribution of the area under the receiver operating characteristic (AUC) for the 100-year return period, within the classification area set for each sub-catchment of the river Po, in Italy. (single-column fitting image)

5.2.4. Map correlation

The MCC is reported here to complement the analysis with a more balanced measure (see subsection 3.2.1. for details) of magnitude and direction of the linear relationship between the hydrogeomorphic delineated flood-prone areas and the flood hazard maps for Europe that can be retrieved from Dottori et al. (2016a-f).

Figures 17 and 18 (see also Figures 26 and 27 in supplementary material) highlight the overall correlation of the maps at the river basin and sub-catchment scales. Results show a positive linear correlation between the hydrogeomorphic flood-prone areas and the reference flood hazard maps. The major European river basins analysed present MCC values around 0.6, with very few basins with values above or below. There is higher heterogeneity at the sub-catchment scale, with most sub-catchments presenting MCC values ranging from 0.4 to 0.6 and very few with values outside this range.

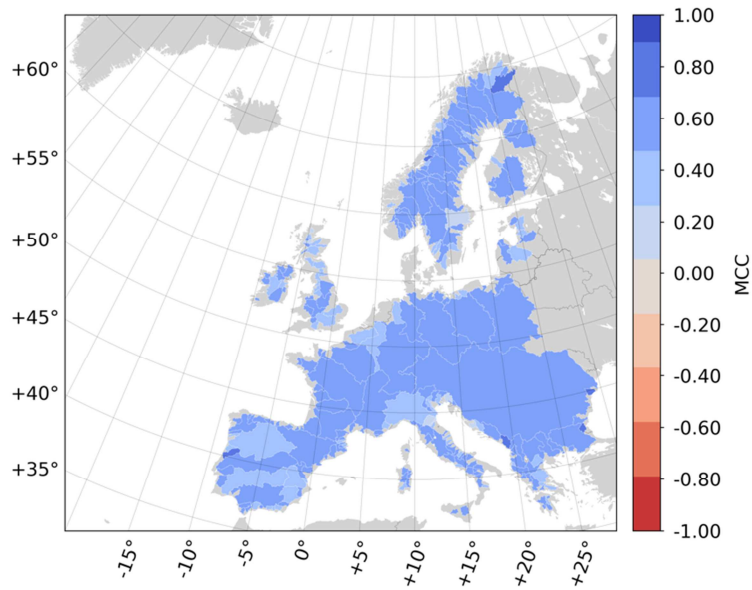


Fig. 17. Spatial distribution of the Mathews Correlation Coefficient (MCC) for the 100-year return period, within the classification area set for each major river basin in Europe. (single-column fitting image)

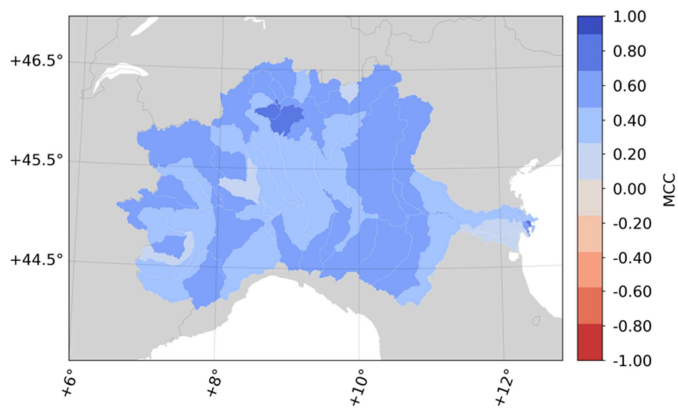


Fig. 18. Spatial distribution of the Mathews Correlation Coefficient (MCC) for the 100-year return period, within the classification area set for each sub-catchment of the river Po, in Italy. (single-column fitting image)

5.2.5. Synthesis of descriptive statistics

To complement the spatial distribution of optimal GFI thresholds and performance measures presented in the previous subsections, and to have a more complete overview of the results, we summarize the data distribution in a set of box plots (Figures 19 and 20). Additional information about the data distribution can be found in supplementary material (tables 2 and 3). Fig. 19 refers to the optimal GFI thresholds obtained by performing the linear binary classification of flood-prone areas within the 270 major river basins of Europe and the 64 sub-catchments of the river Po.

The optimal thresholds of the morphological descriptor GFI present low variability (higher at the sub-catchment scale), with different behaviour in terms of the mean, minima and maxima. The mean GFI thresholds, which tend to fall between 0.20 and 0.23, decrease slightly with return period (see also tables 2 and 3 in supplementary material). This is expected, since the higher the return period, the larger the flood-prone areas and the further the discerning edge moves away from the stream network. Few outliers can be observed outside the upper bound in any of the given scales.

The Youden's J presents low variability at the river basin scale, while at the sub-catchment scale its variability increases significantly. The minima of Youden's J are also significantly lower at the sub-catchment scale. In particular, the mean J value is above 0.64 for all considered return periods at the river basin scale, and above 0.55 at the sub-catchment scale.

Lower variability of the AUC (standard deviation equal to c.a. 0.05) in river basins is observed and remains fairly unchanged across return periods. The AUC at the river basin scale (pan-European level) presents a number of outliers outside the lower bound but higher minima than in sub-catchments of the river Po in Italy. At the sub-catchment scale, there is an increase in variability of the AUC and a slight loss of skill. In general, the AUC mean and median tend to increase with return period at any of the given scales, with average values always above 0.8.

The MCC shows low variability at the river basin scale, taking always positive values with mean above 0.48 at the river basin scale and above 0.46 at the sub-catchment scale.

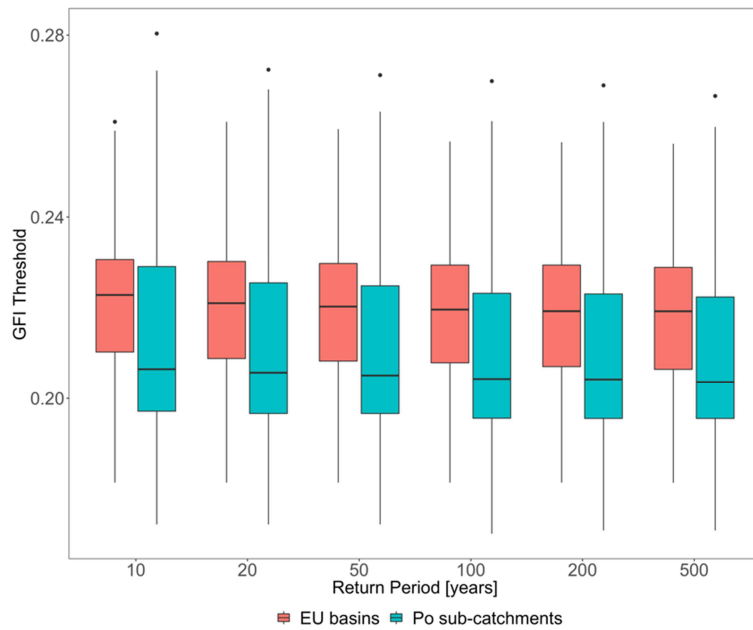


Fig. 19. Data distribution of the optimal Geomorphic Flood Index (GFI) threshold for six return periods. (single-column fitting image)

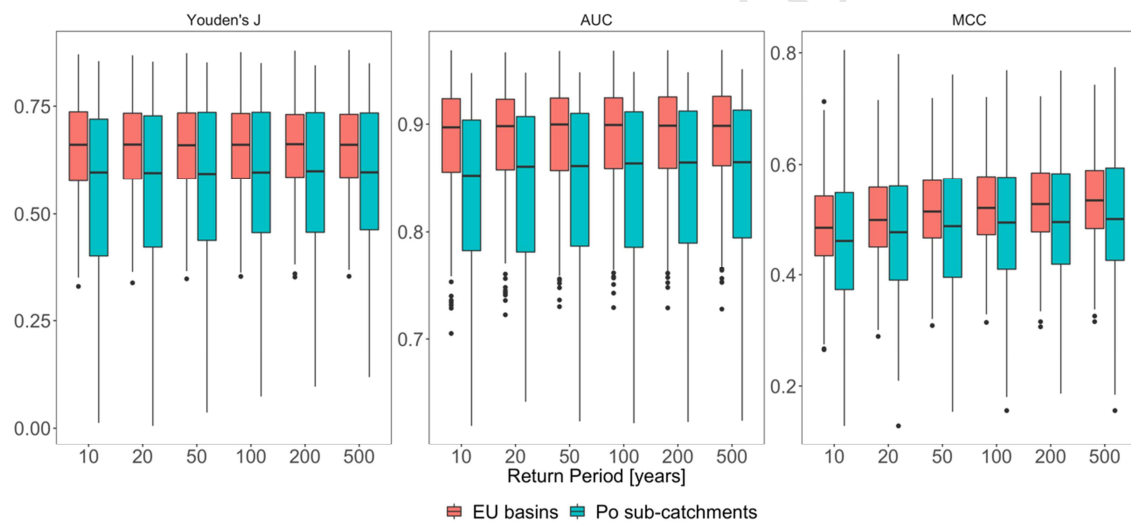


Fig. 20. Data distribution for the Youden's Statistic (J), the area under the receiver operating characteristic (AUC) and the Mathews Correlation Coefficient (MCC) for six return periods. (2-column fitting image)

5.6. Discussion

In this work, we have developed a flood hazard mapping web application based on a data-mining method where the morphological descriptor GFI is used as a classifier of flood-prone areas. Our web application enables users to delineate, downscale and extrapolate flood-prone areas over large scales and we have showcased here its wide spectrum of possible utilizations through an extended analysis at both the European and sub-catchment scale (Po River). The study has been extremely instructive in quantifying the potential of the methodology, its limitations and the critical influence played by input datasets and spatial scales.

The geomorphic classifier threshold was calibrated in terms of the maximum possible Youden's J, obtained by comparing the GFI-derived hydrogeomorphic flood-prone areas with the reference flood hazard maps. This resulted in a homogeneous spatial distribution of the optimal GFI thresholds that decreased with return period, which demonstrates that there is little inter-basin variation and that flood-prone areas actually grow with increasing return periods, as expected. In fact, performances indicate a strong capacity of the GFI to delineate flood-prone areas across return periods, generally achieving high AUC values. We also observed that high AUC values did not always correspond to high MCC values, as the correlation coefficient takes into account the tpr, tnr, fpr and the fnr, because of the additional areas mapped by the hydrogeomorphic web application. Correlation values are nevertheless always positive and relatively high, with few exceptions.

Analyses were carried out on two different datasets: 1) on relatively large river basins of Europe and 2) on a subsample of small catchments of the Po river. Using the first dataset, small changes in performances and calibration parameters were observed; however, moving on to the sub-catchment scale, higher heterogeneity was found. This may have been due to the fact that over larger river basins different morphological features are smoothed out by the classification and the overall outcomes result similar, while within-basin morphological differences may impact the overall performances of the method, which highlights its limitation in specific contexts. Moreover, the method becomes more sensitive to the change of return period of the reference map at the sub-catchment scale. Results suggest that the method should be applied at the basin scale, setting different thresholds within each specific sub-catchment.

The present state of the web application is affected by several approximations that may have an impact on the results. Among others, we should mention:

- pixel size and vertical accuracy of the DEM;
- processing decisions (e.g., de-noising, smoothing and hydrological conditioning);
- channel initiation and stream network definition using a convergent flow model;
- fixed coefficients in the hydraulic scaling relation.

Other factors include differences in the DEMs used to compute the GFI and the reference flood hazard maps. In fact, it would have been more reasonable to compute the GFI layer using the same DEM of the reference, but it was not available. Furthermore, there is a strong possibility that the size of flat areas influences negatively the classification of hydrogeomorphic flood-prone areas. A GFI computed with inadequate horizontal resolution and vertical accuracy will likely underperform in flat areas because of its strong dependency on the elevation difference, but also on the stream network definition, which is known to be problematic in these areas, e.g., Pan et al. (2012). One could also argue that sub-grid scale features, for example embankments, affect performance, particularly in highly anthropized river basins (e.g., river Po, Italy), but we note that such obstacles are not explicitly taken into

consideration neither in the reference flood hazard maps for Europe (see subsection 5.1) nor in the GFI computation.

In spite of the limitations, to be seen as opportunities for further improving the web application, results are very encouraging. We show that European flooded areas for any of the return periods are well approximated by the outputs of the web application. On the one hand, factors affecting performances may be hard to pinpoint and confirm over such large domains, with some issues requiring localized hydraulic studies. However, the clear need for such web technologies and the numerous possibilities that additional datasets and data-driven methods may bring, should motivate a more community-based approach, where such efforts can perhaps be undertaken more coherently and supported consistently. In particular, the development of a web-based system that allows for community interaction may facilitate the current knowledge about flood exposure, while an ensemble of flood hazard maps and studies carried out by a community of users may support hydrogeomorphic flood mapping of higher detail and accuracy.

Finally, we would like to highlight that the hydrogeomorphic flood hazard mapping web application presented in this study could also be used for:

- screening hotspots and elements at risk (e.g., critical infrastructures);
- confirming flood-prone locations with point information (e.g., flood depth) from social media or eye witnessing;
- enhancing remote sensing flood detection (e.g., Westerhoff et al., 2011);
- land use planning.

Users of the web application may well include primary insurers and, to some extent, re-insurers, specialized agencies, civil protection authorities, humanitarian organizations, and asset managers. Further functionality development could include, for example:

- flood depth estimation (Zheng et al., 2018) and risk assessment;
- establishing of statistical relations among the morphological descriptor, climatic and catchment factors (e.g., Jafarzadegan and Merwade, 2017);
- seasonal variability, spatial dependence and spatial heterogeneity of extreme flood events (e.g., Castellarin et al., 2007; Neal et al., 2013);
- estimation of channel and floodplain hydraulic geometries (e.g., Nardi et al., 2006; Andreadis et al., 2013; Zheng et al., 2018) and hydrogeomorphology (Yan et al., 2018);
- the use of other data-mining approaches (Tehrany et al., 2013, 2014; Rahmati and Pourghasem, 2017) to improve the estimation of flood-prone areas.

6. Conclusion

Integrating big open data with data-driven methods and emerging information and communication technologies in flood risk management may well represent a forward step in supporting robust, evidence-based decision-making. Driven by this idea, we have reviewed the progress in simplified hydrogeomorphic methods for the mapping of flood-prone areas, and have adopted and tested – using big open datasets for Europe – a methodology for the classification of flood-prone areas based on a particular morphological descriptor, the GFI. Additionally, we have implemented and described in detail a user-friendly web application, well suited for regional hydrogeomorphic delineation of flood-prone areas, and we have used it to classify and delineate six pan-European hydrogeomorphic flood hazard maps at 25-m pixel resolution (one for each return period: 10, 20, 50, 100, 200 and 500 years) and to

evaluate their quality within major European basins, relative to the flood hazard maps for Europe (Alfieri et al., 2014; Dottori et al., 2016a-f).

We obtained an average efficiency, measured in terms of ROC analysis and AUC of 88.59%. In the analysis focusing on sub-catchments of the river Po in Italy, we obtained an average AUC of 84.23%, in line with results presented in other studies (e.g., Manfreda et al., 2015; Samela et al., 2017). The selected hydrogeomorphic method was found to be valid in replicating, downscaling and extrapolating the flood hazard maps for Europe (Alfieri et al., 2014; Dottori et al., 2016a-f) with different return periods. The hydrogeomorphic flood hazard mapping web application presented in this study provides fast, high-resolution delineations of flood-prone areas over large scales. The web application is currently limited by its I/O capabilities but has the potential to be used as a viable and cost-effective tool for flood risk management.

Acknowledgments

This project has received funding from the *European Union's EU Framework Programme for Research and Innovation Horizon 2020* under Grant Agreement No. 676027.

The authors would like to thank the European Union's Horizon 2020 research and innovation program under the Marie Skłodowska-Curie System-Risk ETN (<https://www.system-risk.eu/>) grant, the *European Union's Earth Observation Programme Copernicus*, Dr. David Tarboton (Utah State University) for TauDEM utilities, the Python Software Foundation for the Python programming language, the Open Source Geospatial Foundation for OpenLayers, MapServer and the GDAL, and the Apache Software Foundation for the Apache HTTP Server. The authors would also like to thank the Editor-in-Chief Dr. Ames and the anonymous reviewers for their thoughtful comments regarding this manuscript. This publication reflects only the authors' views and the European Union is not liable for any use that may be made of the information contained therein.

References

- Alfieri, L., Burek, P., Dutra, E., Krzeminski, B., Muraro, D., Thielen, J., Pappenberger, F., 2012. GloFAS – global ensemble streamflow forecasting and flood early warning. *Hydrology and Earth System Sciences Discussions* 9, 12293–12332. <https://doi.org/10.5194/hessd-9-12293-2012>
- Alfieri, L., Burek, P., Feyen, L., Forzieri, G., 2015. Global warming increases the frequency of river floods in Europe. *Hydrology and Earth System Sciences*, 19, 2247–2260. <https://doi.org/10.5194/hess-19-2247-2015>
- Alfieri, L., Salamon, P., Bianchi, A., Neal, J., Bates, P., Feyen, L., 2014. Advances in pan-European flood hazard mapping. *Hydrological Processes*, 28(13), 4067–4077. <https://doi.org/10.1002/hyp.9947>
- Andreadis, K.M., Schumann, G.J.-P., Pavelsky, T., 2013. A simple global river bankfull width and depth database: Data and Analysis Note. *Water Resources Research*, 49(10), 7164–7168. <https://doi.org/10.1002/wrcr.20440>
- Baker, S.G., Kramer, B.S., 2007. Peirce, Youden, and Receiver Operating Characteristic Curves. *The American Statistician* 61, 343–346. <https://doi.org/10.1198/000313007X247643>
- Baldi, P., Brunak, S., Chauvin, Y., Andersen, C.A., Nielsen, H., 2000. Assessing the accuracy of prediction algorithms for classification: an overview. *Bioinformatics*, 16(5), 209-38. <https://doi.org/10.1093/bioinformatics/16.5.412>
- Barredo, J.I., 2007. Major flood disasters in Europe: 1950-2005. *Natural Hazards*, 42(1), 125–148. <https://doi.org/10.1007/s11069-006-9065-2>

- Bartholmes, J.C., Thielen, J., Ramos, M.H., Gentilini, S., 2009. The European flood alert system EFAS – Part 2: Statistical skill assessment of probabilistic and deterministic operational forecasts. *Hydrol. Earth Syst. Sci.*, 13, 141–153. <https://doi.org/10.5194/hess-13-141-2009>
- Bates, P.D., Horritt, M.S., Fewtrell, T.J., 2010. A simple inertial formulation of the shallow water equations for efficient two-dimensional flood inundation modelling. *Journal of Hydrology*, 387, 33–45. <https://doi.org/10.1016/j.jhydrol.2010.03.027>
- Beven, K.J., Kirkby, M.J., 1979. A physically based, variable contributing area model of basin hydrology. *Hydrological Sciences Bulletin*, 24(1), 43–69. <https://doi.org/10.1080/02626667909491834>
- Bhowmik, N.G., 1984. Hydraulic geometry of floodplains. *Journal of Hydrology*, 68(1–4), 369–374, 377–401. [https://doi.org/10.1016/0022-1694\(84\)90221-X](https://doi.org/10.1016/0022-1694(84)90221-X)
- Bley, S., Deneke, S., 2013. A threshold-based cloud mask for the high-resolution visible channel of Meteosat Second Generation SEVERI. *Atmos. Meas. Tech.*, 6. <https://doi.org/10.5194/amt-6-2713-2013>
- Bradley, A.P., 1997. The use of the area under the ROC curve in the evaluation of machine learning algorithms. *Pattern Recognition*, 30(7), 1145–1159. [https://doi.org/10.1016/S0031-3203\(96\)00142-2](https://doi.org/10.1016/S0031-3203(96)00142-2)
- Castellarin, A., Vogel, R.M., Matalas, N.C., 2007. Multivariate probabilistic regional envelopes of extreme floods. *Journal of Hydrology* 336, 376–390. <https://doi.org/10.1016/j.jhydrol.2007.01.007>
- Degiorgis, M., Gnecco, G., Gorni, S., Roth, G., Sanguineti, M., Taramasso, A. C., 2012. Classifiers for the detection of flood-prone areas using remote sensed elevation data. *Journal of Hydrology*, 470–471, 302–315. <https://doi.org/10.1016/j.jhydrol.2012.09.006>
- de Jager, A.L., Vogt, J.V., 2010. Development and demonstration of a structured hydrological feature coding system for Europe. *Hydrological Sciences Journal*, 55(5), 661–675. <https://doi.org/10.1080/02626667.2010.490786>
- Demir, I., Krajewski, W.F., 2013. Towards an integrated Flood Information System: Centralized data access, analysis, and visualization. *Environmental Modelling & Software* 50, 77–84. <https://doi.org/10.1016/j.envsoft.2013.08.009>
- Dodov, B., Fofoula-Georgiou, E., 2005. Fluvial processes and streamflow variability: interplay in the scale-frequency continuum and implications for scaling. *Water Resources Research*, 41(5), W05005. <https://doi.org/10.1029/2004WR003408>
- Dodov, B.A., Fofoula-Georgiou, E., 2006. Floodplain morphometry extraction from a high-resolution digital elevation model: a simple algorithm for regional analysis studies. *IEEE Geoscience and Remote Sensing Letters*, 3(3), 410–413. <https://doi.org/10.1109/LGRS.2006.874161>
- [Dataset] Dottori, F., Alfieri, L., Salamon, P., Bianchi, A., Feyen, L., Lorini, V., 2016a. Flood hazard map for Europe, 10-year return period. European Commission, Joint Research Centre (JRC) PID: http://data.europa.eu/89h/jrc-floods-floodmapeu_rp10y-tif
- [Dataset] Dottori, F., Alfieri, L., Salamon, P., Bianchi, A., Feyen, L., Lorini, V., 2016b. Flood hazard map for Europe, 20-year return period. European Commission, Joint Research Centre (JRC) PID: http://data.europa.eu/89h/jrc-floods-floodmapeu_rp20y-tif
- [Dataset] Dottori, F., Alfieri, L., Salamon, P., Bianchi, A., Feyen, L., Lorini, V., 2016c. Flood hazard map for Europe, 50-year return period. European Commission, Joint Research Centre (JRC) PID: http://data.europa.eu/89h/jrc-floods-floodmapeu_rp50y-tif
- [Dataset] Dottori, F., Alfieri, L., Salamon, P., Bianchi, A., Feyen, L., Lorini, V., 2016d. Flood hazard map for Europe, 100-year return period. European Commission, Joint Research Centre (JRC) PID: http://data.europa.eu/89h/jrc-floods-floodmapeu_rp100y-tif

- [Dataset] Dottori, F., Alfieri, L., Salamon, P., Bianchi, A., Feyen, L., Lorini, V., 2016e. Flood hazard map for Europe, 200-year return period. European Commission, Joint Research Centre (JRC) PID: http://data.europa.eu/89h/jrc-floods-floodmapeu_rp200y-tif
- [Dataset] Dottori, F., Alfieri, L., Salamon, P., Bianchi, A., Feyen, L., Lorini, V., 2016f. Flood hazard map for Europe, 500-year return period. European Commission, Joint Research Centre (JRC) PID: http://data.europa.eu/89h/jrc-floods-floodmapeu_rp500y-tif
- Dottori, F., Salamon, P., Bianchi, A., Alfieri, L., Hirpa, F.A., Feyen, L., 2016. Development and evaluation of a framework for global flood hazard mapping. *Advances in Water Resources* 94, 87–102. <https://doi.org/10.1016/j.advwatres.2016.05.002>
- [Dataset] EC-JRC, 2008. Catchment Characterisation and Modelling (CCM, Version 2.1). European Commission, Joint Research Centre (JRC). Available at: <http://ccm.jrc.ec.europa.eu/> (Accessed 1 October 2016).
- [Dataset] EEA, 2015. Copernicus Land Monitoring Service, European Digital Elevation Model (EU-DEM, Version 1.0). European Environment Agency. Available at: <http://land.copernicus.eu/pan-european/satellite-derived-products/eu-dem/> (Accessed 1 May 2018).
- EEA, 2016. Flood risks and environmental vulnerability: Exploring the synergies between floodplain restoration, water policies and thematic policies. EEA Report No. 1/2016, European Environment Agency, Copenhagen, Denmark, pp. 84. <https://www.eea.europa.eu/publications/flood-risks-and-environmental-vulnerability>
- EU, 2007. Directive 2007/60/EC of the European Parliament and of the Council on the assessment and management of flood risks. *Official Journal of the European Union*, L 288/27, 186–193. <https://eur-lex.europa.eu/legal-content/EN/TXT/?uri=CELEX:32007L0060>
- Fawcett, T., 2006. An introduction to ROC analysis. *Pattern Recognition Letters*, 27(8), 861–874. <https://doi.org/10.1016/j.patrec.2005.10.010>
- Gharari, S., Hrachowitz, M., Fenicia, F., Savenije, H.H.G., 2011. Hydrological landscape classification: investigating the performance of HAND based landscape classifications in a central European meso-scale catchment. *Hydrology and Earth System Sciences* 15, 3275–3291. <https://doi.org/10.5194/hess-15-3275-2011>
- Giannoni, F., Roth, G., Rudari, R., 2005. A procedure for drainage network identification from geomorphology and its application to the prediction of the hydrologic response. *Advances in Water Resources*, 28(6), 567–581. <https://doi.org/10.1016/j.advwatres.2004.11.013>
- Gorelick, N., Hancher, M., Dixon, M., Ilyushchenko, S., Thau, D., Moore, R., 2017. Google Earth Engine: Planetary-scale geospatial analysis for everyone. *Remote Sensing of Environment* 202, 18–27. <https://doi.org/10.1016/j.rse.2017.06.031>
- Jafarzadegan, K., Merwade, V., 2017. A DEM-based approach for large-scale floodplain mapping in ungauged watersheds. *Journal of Hydrology*, 550, 650–662. <https://doi.org/10.1016/j.jhydrol.2017.04.053>
- Jongman, B., Hochrainer-Stigler, S., Feyen, L., Aerts, J.J.H., Mechler, R., Wouter Botzen, W.J., Bouwer, L. M., Pflug, G., Rojas, R., Ward, P.J., 2014. Increasing stress on disaster-risk finance due to large floods. *Nature Climate Change*, 4, 264–268. <https://doi.org/10.1038/nclimate2124>
- Kochilakis, G., Poursanidis, D., Chrysoulakis, N., Varella, V., Kotroni, V., Eftychidis, G., Lagouvardos, K., Papathanasiou, C., Karavokyros, G., Aivazoglou, M., Makropoulos, C., Mimikou, M., 2016. A web based DSS for the management of floods and wildfires (FLIRE) in urban and periurban areas. *Environmental Modelling & Software* 86, 111–115. <https://doi.org/10.1016/j.envsoft.2016.09.016>
- Kotteck, M., Grieser, J., Beck, C., Rudolf, B., Rubel, F., 2006. World Map of the Köppen-Geiger climate classification updated. *Meteorologische Zeitschrift*, 15(3), 259–263. <https://doi.org/10.1127/0941-2948/2006/0130>

- Kubat, M., Holte, R. C., Matwin, S., 1998. Machine Learning for the Detection of Oil Spills in Satellite Radar Images. *Machine Learning*, 30, 195-215.
<https://doi.org/10.1023/A:1007452223027>
- Leopold, L.B., Maddock, T., 1953. The hydraulic geometry of stream channels and some physiographic implications. USGS Professional Paper 252, United States Geological Survey, Washington, D.C., United States of America, pp. 57.
<https://pubs.er.usgs.gov/publication/pp252>
- Leskens, J.G., Brugnach, M., Hoekstra, A.Y., Schuurmans, W., 2014. Why are decisions in flood disaster management so poorly supported by information from flood models? *Environmental Modelling & Software* 53, 53–61.
<https://doi.org/10.1016/j.envsoft.2013.11.003>
- Manfreda, S., Di Leo, M., Sole, A., 2011. Detection of flood-prone areas using digital elevation models. *Journal of Hydrologic Engineering*, 16(10), 781–790.
[https://doi.org/10.1061/\(ASCE\)HE.1943-5584.0000367](https://doi.org/10.1061/(ASCE)HE.1943-5584.0000367)
- Manfreda, S., Nardi, F., Samela, C., Grimaldi, S., Taramasso, A.C., Roth, G., Sole, A., 2014. Investigation on the use of geomorphic approaches for the delineation of flood prone areas. *Journal of Hydrology*, 517, 863–876.
<https://doi.org/10.1016/j.jhydrol.2014.06.009>
- Manfreda, S., Samela, C., Gioia, A., Consoli, G.G., Iacobellis, V., Giuzio, L., Cantisani, A., Sole, A. 2015. Flood-prone areas assessment using linear binary classifiers based on flood maps obtained from 1D and 2D hydraulic models. *Natural Hazards*, 79(2), 735–754. <https://doi.org/10.1007/s11069-015-1869-5>
- Manzato, A., 2007. A Note On the Maximum Peirce Skill Score. *Weather and Forecasting* 22, 1148–1154. <https://doi.org/10.1175/WAF1041.1>
- Matthews, B.W., 1975. Comparison of the predicted and observed secondary structure of T4 phage lysozyme. *Biochimica et Biophysica Acta*, 405(2), 442–451.
[https://doi.org/10.1016/0005-2795\(75\)90109-9](https://doi.org/10.1016/0005-2795(75)90109-9)
- Ma, Y., Wu, H., Wang, L., Huang, B., Ranjan, R., Zomaya, A., Jie, W., 2015. Remote sensing big data computing: Challenges and opportunities. *Future Generation Computer Systems*, 51, 47–60. <https://doi.org/10.1016/j.future.2014.10.029>
- Montgomery, D.R., Dietrich, W.E., 1989. Source areas drainage density and channel initiation. *Water Resources Research*, 25(8), 1907–1918.
<https://doi.org/10.1029/WR025i008p01907>
- Muis, S., Guneralp, B., Jongman, B., Aerts, J.C.J.H., Ward, P.J., 2015. Flood risk and adaptation strategies under climate change and urban expansion: A probabilistic analysis using global data. *Sci. Total Environ.*, 538, 445–457.
<https://doi.org/10.1016/j.scitotenv.2015.08.068>
- Nardi, F., Vivoni, E. R., Grimaldi, S., 2006. Investigating a floodplain scaling relation using a hydrogeomorphic delineation method. *Water Resources Research*, 42(9), W09409.
<https://doi.org/10.1029/2005WR004155>
- Neal, J., Keef, C., Bates, P., Beven, K., Leedal, D., 2013. Probabilistic flood risk mapping including spatial dependence. *Hydrological Processes*, 27, 1349–1363.
<https://doi.org/10.1002/hyp.9572>
- Neal, J., Schumann, G., Bates, P., 2012. A subgrid channel model for simulating river hydraulics and floodplain inundation over large and data sparse areas. *Water Resources Research* 48(11), W11506. <https://doi.org/10.1029/2012WR012514>
- Neal, J., Villanueva, I., Wright, N., Willis, T., Fewtrell, T., Bates, P., 2012. How much physical complexity is needed to model flood inundation? *Hydrological Processes*, 26, 2264–2282. <https://doi.org/10.1002/hyp.8339>
- Nobre, A.D., Cuartas, L.A., Momo, M.R., Severo, D.L., Pinheiro, A., Nobre, C.A., 2016. HAND contour: a new proxy predictor of inundation extent. *Hydrological Processes*, 30(2), 320–333. <https://doi.org/10.1002/hyp.10581>
- OSGeo, 2017. Geospatial Data Abstraction Library (GDAL, Version 2.2.3), Open Source Geospatial Foundation. Available at: <http://www.gdal.org/> (Accessed 1 May 2018).

- Pan, F., Stieglitz, M., McKane, R.B., 2012. An algorithm for treating flat areas and depressions in digital elevation models using linear interpolation. *Water Resources Research*, 48(6), 1–13. <https://doi.org/10.1029/2011WR010735>
- Pappenberger, F., Cloke, H.L., Parker, D.J., Wetterhall, F., Richardson, D.S., Thielen, J., 2015. The monetary benefit of early flood warnings in Europe. *Environmental Science Policy*, 51, 278–291. <https://doi.org/10.1016/j.envsci.2015.04.016>
- Peirce, C. S., 1884: The numerical measure of the success of pre- dictions. *Science*, 4, 453–454. <https://doi.org/10.1126/science.ns-4.93.453-a>
- Rahmati, O., Kornejady, A., Samadi, M., Nobre, A.D., Melesse, A.M., 2018. Development of an automated GIS tool for reproducing the HAND terrain model. *Environmental Modelling & Software* 102, 1–12. <https://doi.org/10.1016/j.envsoft.2018.01.004>
- Rahmati, O., Pourghasemi, H.R., 2017. Identification of Critical Flood Prone Areas in Data-Scarce and Ungauged Regions: A Comparison of Three Data Mining Models. *Water Resources Management* 31, 1473–1487. <https://doi.org/10.1007/s11269-017-1589-6>
- Rajib, M.A., Merwade, V., Kim, I.L., Zhao, L., Song, C., Zhe, S., 2016. SWATShare – A web platform for collaborative research and education through online sharing, simulation and visualization of SWAT models. *Environmental Modelling & Software* 75, 498–512. <https://doi.org/10.1016/j.envsoft.2015.10.032>
- Rennó, C.D., Nobre, A.D., Cuartas, L.A., Soares, J.V., Hodnett, M.G., Tomasella, J., Waterloo, M.J., 2008. HAND, a new terrain descriptor using SRTM-DEM: Mapping terra-firme rainforest environments in Amazonia. *Remote Sensing of Environment*, 112(9), 3469–3481. <https://doi.org/10.1016/j.rse.2008.03.018>
- Samela, C., Manfreda, S., De Paola, F., Giugni, M., Sole, A., Fiorentino, M., 2016. DEM-based approaches for the delineation of flood-prone areas in an ungauged basin in Africa. *Journal of Hydrologic Engineering*, 21(2), 06015010. [https://doi.org/10.1061/\(ASCE\)HE.1943-5584.0001272](https://doi.org/10.1061/(ASCE)HE.1943-5584.0001272)
- Samela, C., Troy, T.J., Manfreda, S., 2017. Geomorphic classifiers for flood-prone areas delineation for data-scarce environments. *Advances in Water Resources*, 102, 13–28. <https://doi.org/10.1016/j.advwatres.2017.01.007>
- Schumann, G.J.-P., Andreadis, K.M., Bates, P.D., 2014. Downscaling coarse grid hydrodynamic model simulations over large domains. *Journal of Hydrology* 508, 289–298. <https://doi.org/10.1016/j.jhydrol.2013.08.051>
- Schumann, G.J.-P., Vernieuwe, H., De Baets, B., Verhoest, N.E.C., 2014. ROC-based calibration of flood inundation models. *Hydrological Processes*, 28(22), 5495–5502. <https://doi.org/10.1002/hyp.10019>
- Şen, O., Kahya, E., 2017. Determination of flood risk: A case study in the rainiest city of Turkey. *Environmental Modelling & Software* 93, 296–309. <https://doi.org/10.1016/j.envsoft.2017.03.030>
- Stephenson, D.B., 2000. Use of the “Odds Ratio” for Diagnosing Forecast Skill. *Weather and Forecasting* 15, 221–232. [https://doi.org/10.1175/1520-0434\(2000\)015<0221:UOTORF>2.0.CO;2](https://doi.org/10.1175/1520-0434(2000)015<0221:UOTORF>2.0.CO;2)
- Strahler, A.N., 1964. *Handbook of Applied Hydrology*, edited by Chow, V.T., 4–39, 4–76, McGraw-Hill, New York.
- Swain, N.R., Christensen, S.D., Snow, A.D., Dolder, H., Espinoza-Dávalos, G., Goharian, E., Jones, N.L., Nelson, E.J., Ames, D.P., Burian, S.J., 2016. A new open source platform for lowering the barrier for environmental web app development. *Environmental Modelling & Software* 85, 11–26. <https://doi.org/10.1016/j.envsoft.2016.08.003>
- Swain, N.R., Latu, K., Christensen, S.D., Jones, N.L., Nelson, E.J., Ames, D.P., Williams, G.P., 2015. A review of open source software solutions for developing water resources web applications. *Environmental Modelling & Software* 67, 108–117. <https://doi.org/10.1016/j.envsoft.2015.01.014>
- Swets, J.A., 1973. The Relative Operating Characteristic in Psychology 182, 11. <https://doi.org/10.1126/science.182.4116.990>

- Swets, J.A., 1988. Measuring the accuracy of diagnostic systems. *Science*, 240(4867), 1285–1293. <https://doi.org/10.1126/science.3287615>
- Tarboton, D., 2015. *Terrain Analysis Using Digital Elevation Models (TauDEM, Version 5)*. Hydrology Research Group, Utah State University. Available at: <http://hydrology.usu.edu/taudem/taudem5/> (Accessed 1 May 2018).
- [Dataset] USGS, 2015. Shuttle Radar Topography Mission (SRTM) 1 Arc-Second Global. United States Geological Survey. Available at: <https://lta.cr.usgs.gov/SRTM1Arc> (Accessed 1 May 2018).
- Tehrany, M.S., Pradhan, B., Jebur, M.N., 2013. Spatial prediction of flood susceptible areas using rule based decision tree (DT) and a novel ensemble bivariate and multivariate statistical models in GIS. *Journal of Hydrology* 504, 69–79. <https://doi.org/10.1016/j.jhydrol.2013.09.034>
- Tehrany, M.S., Pradhan, B., Jebur, M.N., 2014. Flood susceptibility mapping using a novel ensemble weights-of-evidence and support vector machine models in GIS. *Journal of Hydrology* 512, 332–343. <https://doi.org/10.1016/j.jhydrol.2014.03.008>
- Ward, P.J., Jongman, B., Salamon, P., Simpson, A., Bates, P., De Groeve, T., Muis, S., Coughlan de Perez, E., Rudari, R., Trigg, M.A., Winsemius, H.C., 2015. Usefulness and limitations of global flood risk models. *Nature Climate Change*, 5, 712–715. <https://doi.org/10.1038/nclimate2742>
- Van Der Knijff, J.M., Younis, J., De Roo, A.P.J., 2010. LISFLOOD: a GIS-based distributed model for river basin scale water balance and flood simulation. *International Journal of Geographical Information Science*, 24, 189–212. <https://doi.org/10.1080/13658810802549154>
- Westerhoff, R.S., Kleuskens, M.P.H., Winsemius, H.C., Huizinga, H.J., Brakenridge, G.R., Bishop, C., 2013. Automated global water mapping based on wide-swath orbital synthetic-aperture radar. *Hydrology and Earth System Sciences* 17, 651–663. <https://doi.org/10.5194/hess-17-651-2013>
- Williams, W.A., Jensen, M.E., Chris Winne, J., Redmond, R.L., 2000. An automated technique for delineating and characterizing valley-bottom settings. *Environmental monitoring and assessment*, 64(1), 105–114. <https://doi.org/10.1023/A:1006471427421>
- Yan, Q., Iwasaki, T., Stumpf, A., Belmont, P., Parker, G., Kumar, P., 2018. Hydrogeomorphological differentiation between floodplains and terraces. *Earth Surface Processes and Landforms*, 43, 218–228. <https://doi.org/10.1002/esp.4234>
- Youden, W.J., 1950. Index for rating diagnostic tests. *Cancer*, 3(1), 32–35. [https://doi.org/10.1002/1097-0142\(1950\)3:1<32::AID-CNCR2820030106>3.0.CO;2-3](https://doi.org/10.1002/1097-0142(1950)3:1<32::AID-CNCR2820030106>3.0.CO;2-3)
- Zheng, X., Tarboton, D.G., Maidment, D.R., Liu, Y.Y., Passalacqua, P., 2018. River Channel Geometry and Rating Curve Estimation Using Height above the Nearest Drainage. *JAWRA Journal of the American Water Resources Association* 54, 785–806. <https://doi.org/10.1111/1752-1688.12661>
- Ågren, A.M., Lidberg, W., Strömberg, M., Ogilvie, J., Arp, P.A., 2014. Evaluating digital terrain indices for soil wetness mapping – a Swedish case study. *Hydrol. Earth Syst. Sci.*, 18, 3623–3634. <https://doi.org/10.5194/hess-18-3623-2014>

Supplementary material

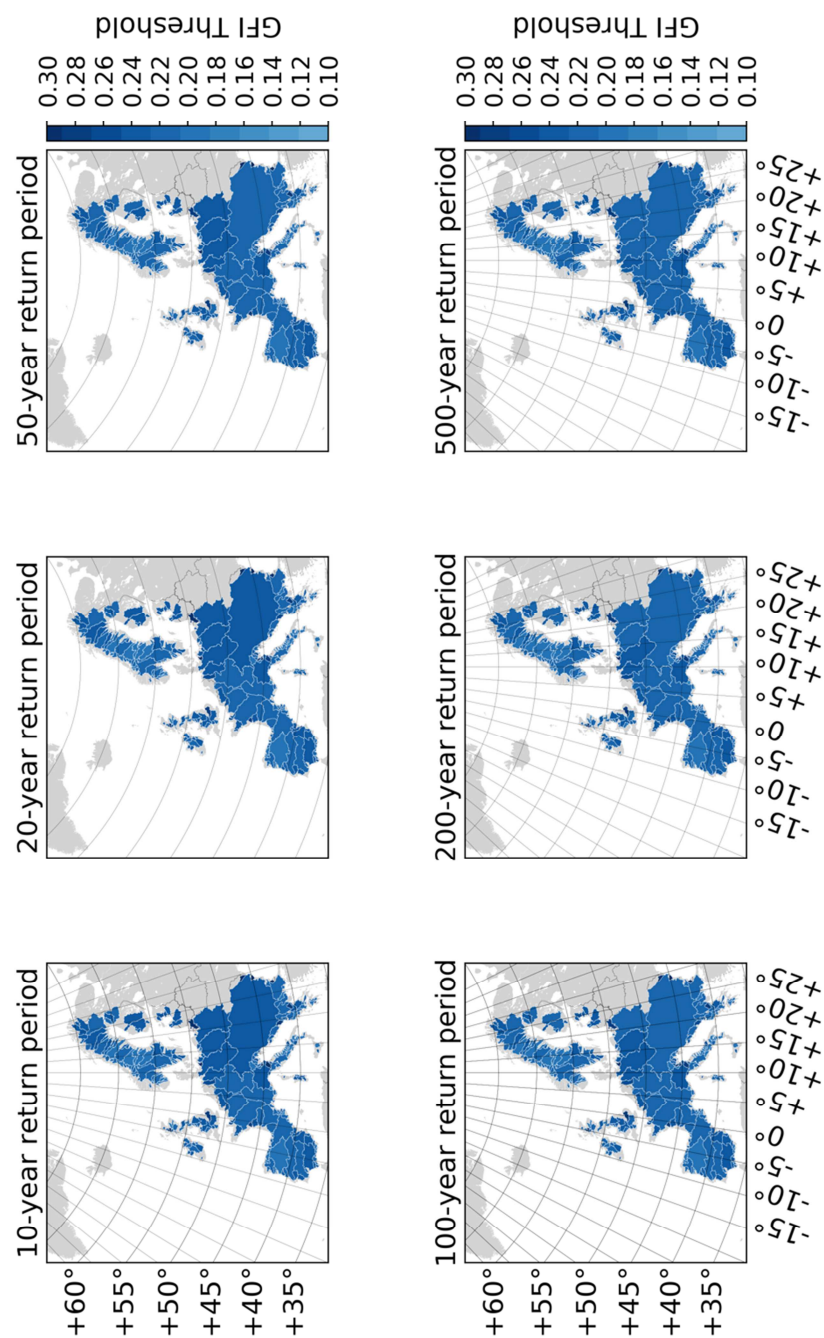


Fig. 21. Spatial distribution of the optimal Geomorphic Flood Index (GFI) threshold for six return periods, within the classification area set for each major river basin in Europe. (2-column fitting image)

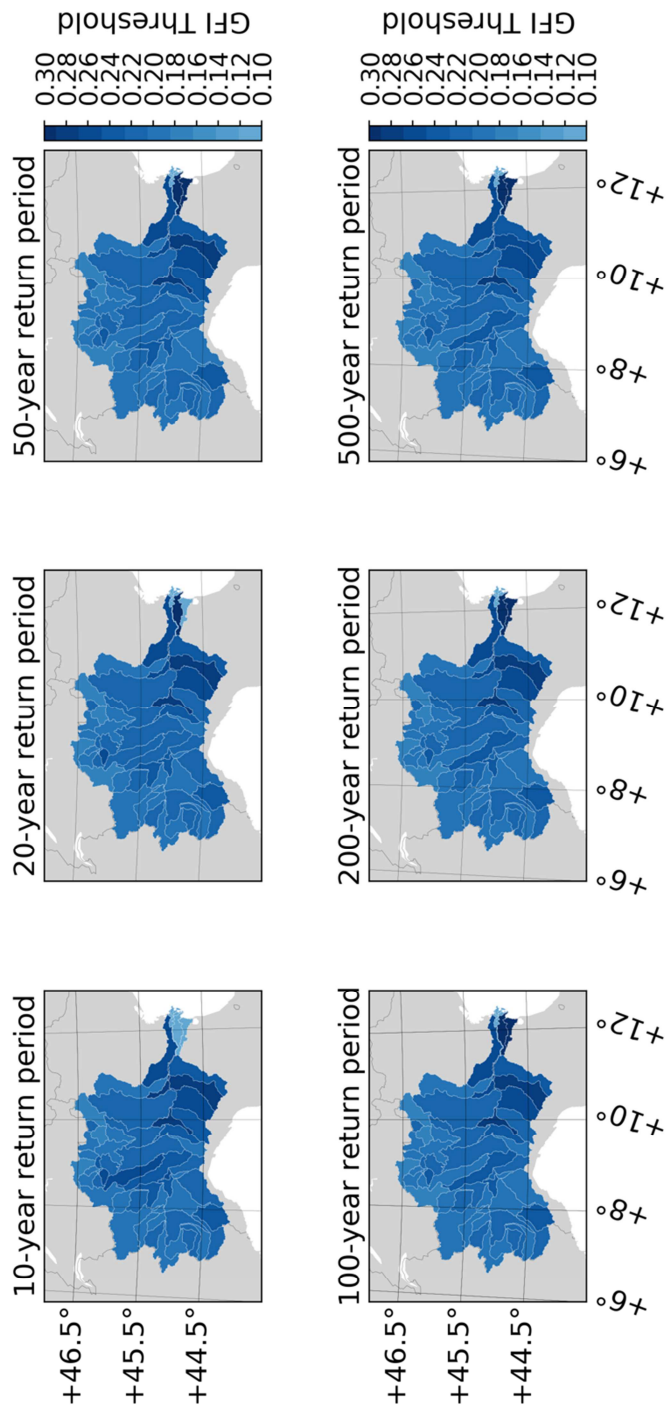


Fig. 22. Spatial distribution of the optimal Geomorphic Flood Index (GFI) threshold for six return periods, within the classification area set for each sub-catchment of the river Po, in Italy. (2-column fitting image)

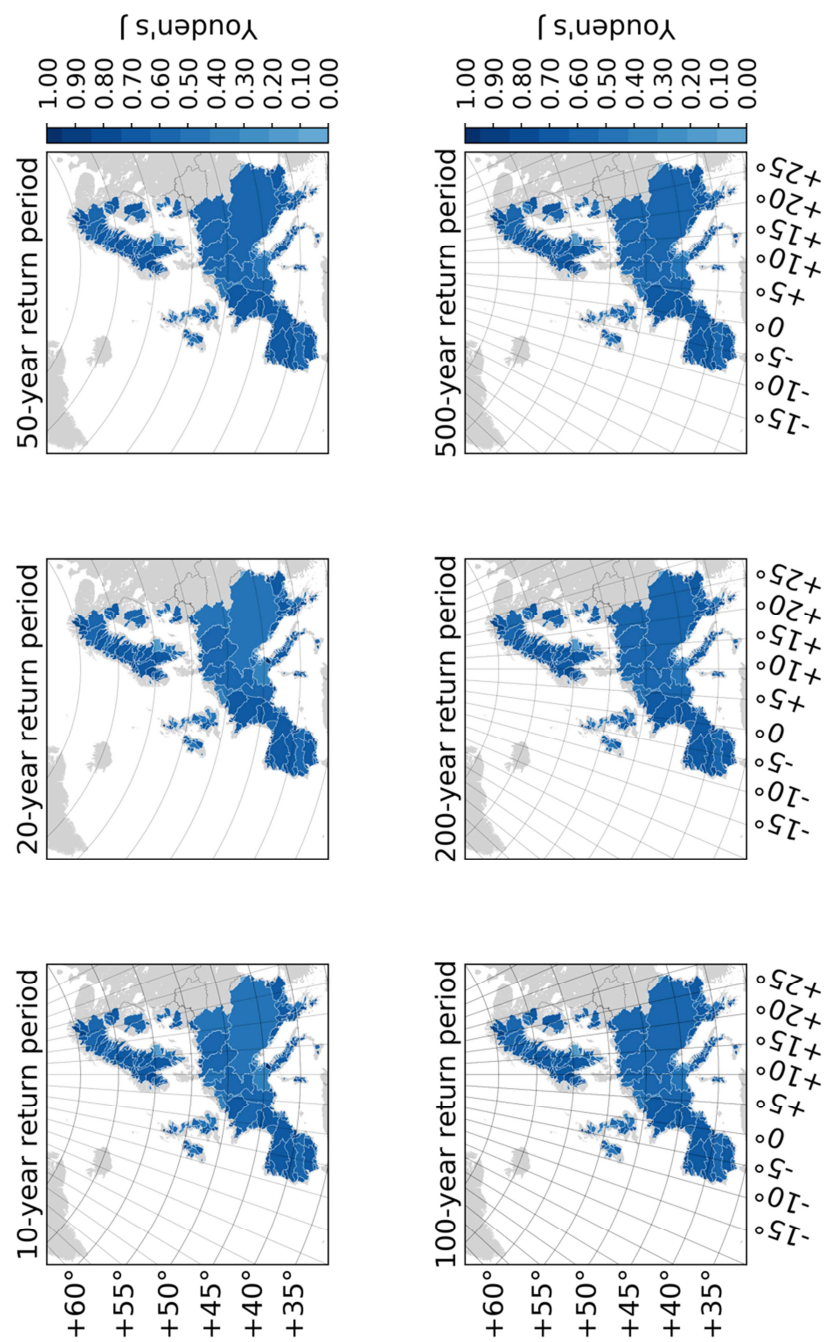


Fig. 23. Spatial distribution of the Youden's statistic (J) for six return periods, within the classification area set for each major river basin in Europe. (2-column fitting image)

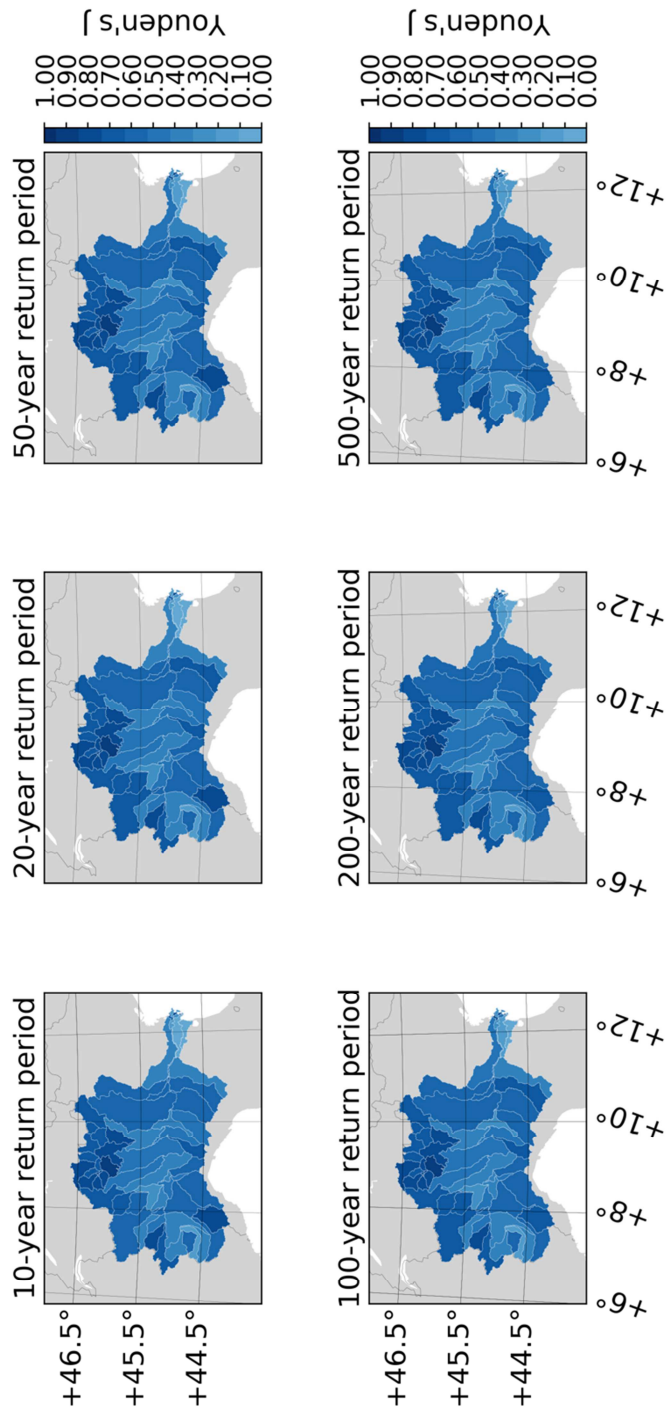


Fig. 24. Spatial distribution of the Youden's statistic (J) for six return periods, within the classification area set for each sub-catchment of the river Po, in Italy. (2-column fitting image)

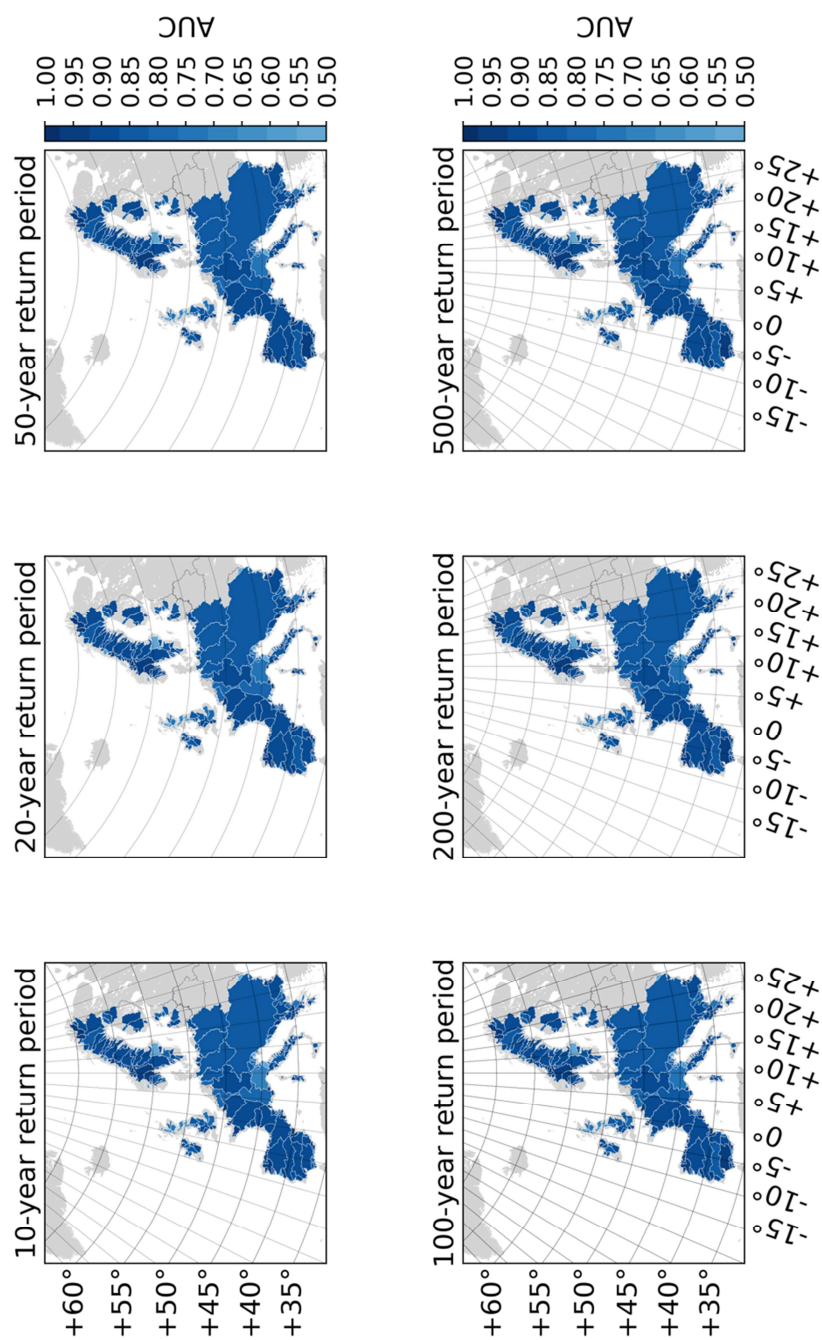


Fig. 25. Spatial distribution of the area under the receiver operating characteristic (AUC) for six return periods, within the classification area set for each major river basin in Europe. (2-column fitting image)

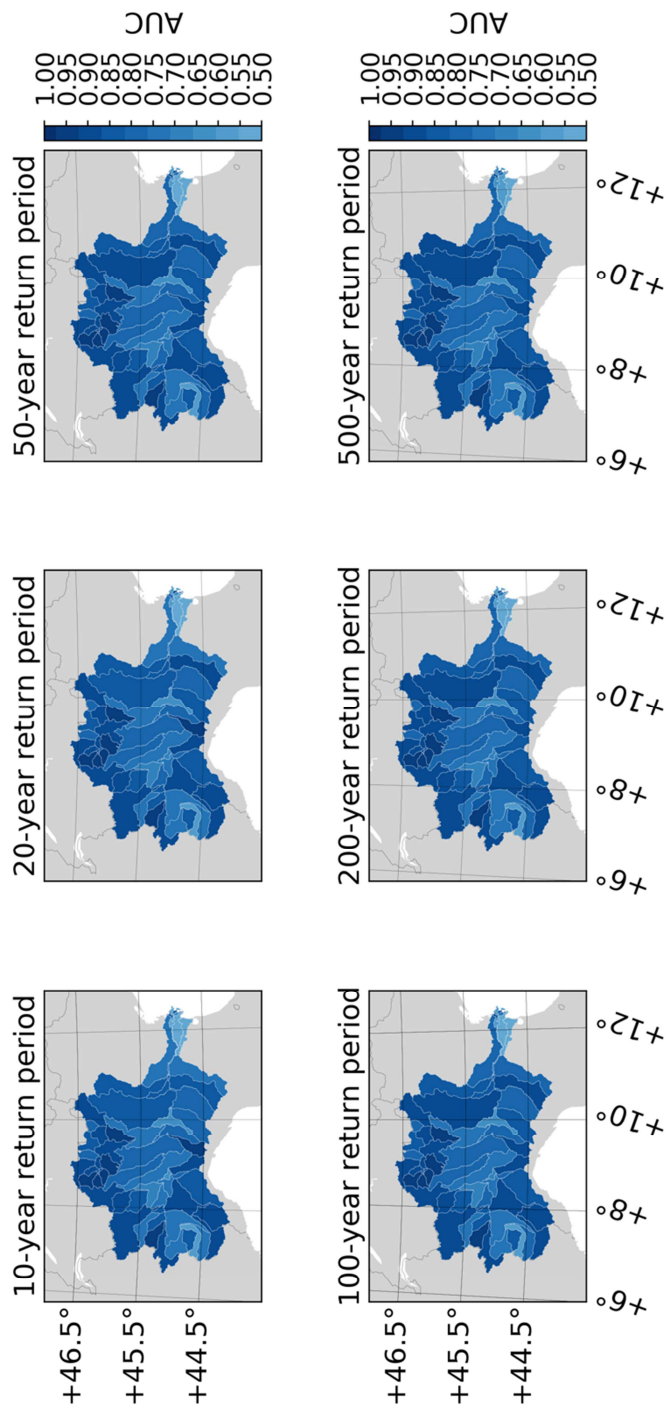


Fig. 26. Spatial distribution of the area under the receiver operating characteristic (AUC) for six return periods, within the classification area set for each sub-catchment of the river Po, in Italy. (2-column fitting image)

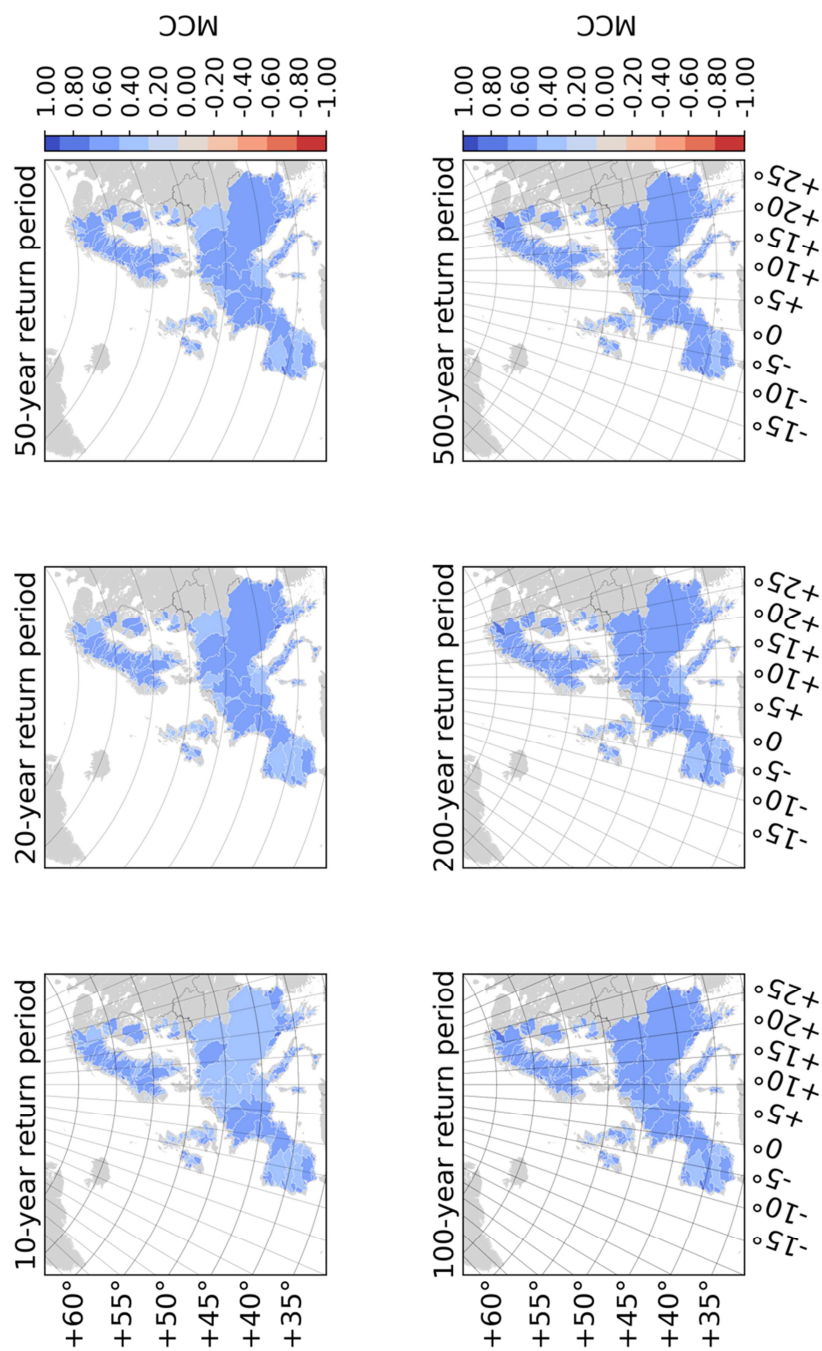


Fig. 27. Spatial distribution of the Mathews correlation coefficient (MCC) for six return periods, within the classification area set for each major river basin in Europe. (2-column fitting image)

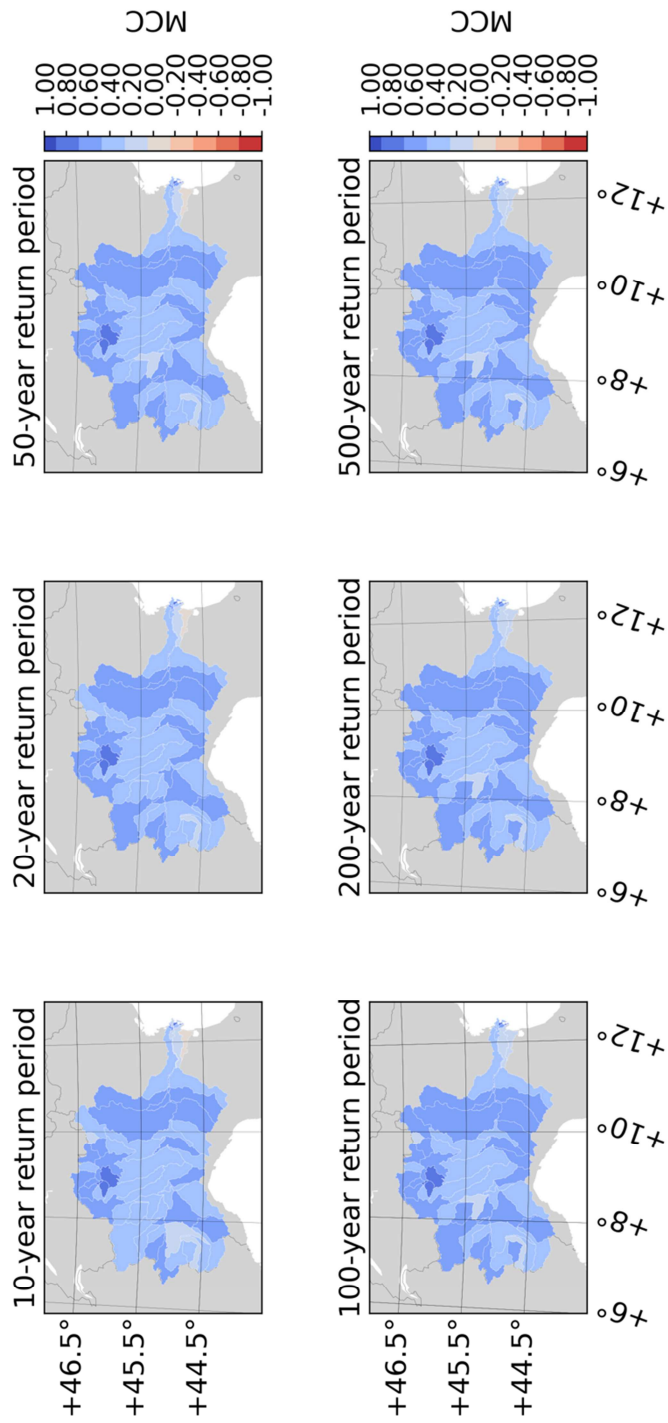


Fig. 28. Spatial distribution of the Mathews Correlation Coefficient (MCC) for six return periods, within the classification area set for each sub-catchment of the river Po, in Italy. (2-column fitting image)

Table 2

Summary statistics for the area under the receiver operating characteristic (AUC), the optimal geomorphic flood index (GFI) threshold, the Youden's Statistic (J) and the Mathews Correlation Coefficient (MCC) across major river basins in Europe and return periods. (two-column fitting table)

		Return Period [years]					
		10	20	50	100	200	500
J	mean	0.6499	0.6514	0.6520	0.6529	0.6531	0.6533
	median	0.6615	0.6619	0.6604	0.6615	0.6628	0.6614
	standard deviation	0.1127	0.1104	0.1086	0.1074	0.1067	0.1063
GFI Thresholds	mean	0.2208	0.2199	0.2192	0.2186	0.2181	0.2175
	median	0.2227	0.2209	0.2202	0.2195	0.2192	0.2192
	standard deviation	0.0143	0.0143	0.0144	0.0143	0.0144	0.0145
AUC	mean	0.8829	0.8845	0.8858	0.8867	0.8873	0.8879
	median	0.8971	0.8982	0.8997	0.8992	0.8986	0.8985
	standard deviation	0.0536	0.0518	0.0504	0.0496	0.0491	0.0487
MCC	mean	0.4868	0.5017	0.5145	0.5223	0.5282	0.5339
	median	0.4861	0.4999	0.5147	0.5213	0.5281	0.5350
	standard deviation	0.0813	0.0798	0.0798	0.0786	0.0795	0.0803

Table 3

Summary statistics for the area under the receiver operating characteristic (AUC), the optimal Geomorphic Flood Index (GFI) threshold, the Youden's Statistic (J) and the Mathews Correlation Coefficient (MCC) across the sub-catchments of the river Po, in Italy, and return periods. (two-column fitting table)

		Return Period [years]					
		10	20	50	100	200	500
J	mean	0.5599	0.5648	0.5715	0.5744	0.5768	0.5785
	median	0.5978	0.5962	0.5942	0.5977	0.6006	0.5982
	standard deviation	0.1983	0.1957	0.1904	0.1868	0.1845	0.1832
GFI Thresholds	mean	0.2139	0.2117	0.2104	0.2095	0.2093	0.2089
	median	0.2066	0.2058	0.2052	0.2044	0.2043	0.2037
	standard deviation	0.0259	0.0241	0.0230	0.0227	0.0225	0.0223
AUC	mean	0.8373	0.8397	0.8426	0.8437	0.8447	0.8457
	median	0.8527	0.8610	0.8616	0.8641	0.8649	0.8652
	standard deviation	0.0799	0.0788	0.0770	0.0768	0.0764	0.0762
MCC	mean	0.4740	0.4820	0.4910	0.4947	0.4996	0.5032
	median	0.4654	0.4777	0.4885	0.4950	0.4945	0.5013
	standard deviation	0.1286	0.1290	0.1299	0.1291	0.1290	0.1294

video_01.mp4

MMC 1. Video walkthrough of the web application hydrogeomorphic flood analyzer integrated in the SmartFLOOD platform.

video_02.mp4

MMC 2. Video walkthrough of the Geographic Information System (GIS) interface of web application hydrogeomorphic flood analyzer integrated in the SmartFLOOD platform.

floodhazard_gfi-baf789bb693a.tar.gz (<http://dx.doi.org/10.17632/pcxmm2hnfw.1>)

Software 1. Implementation of the Geomorphic Flood Index (GFI) classification workflow in Python programming language. Desktop version with instructions for compiling and test cases included.

Highlights

- Progress in hydrogeomorphic flood hazard mapping is presented.
- A cloud-based web application for data-driven hydrogeomorphic flood hazard mapping is implemented.
- The GFI classifier displayed strong discerning capabilities for mapping flood-prone areas with an average area under the receiver operating characteristic curve of approximately 88% within major river basins in Europe.
- Flood-prone areas for the whole Europe are computed and evaluated for different return periods using the proposed web application.